Zhou et al. Annals of Forest Science (2025) 82:20
https://doi.org/10.1186/s13595-025-01291-w

Annals of Forest Science

RESEARCH PAPER

Open Access

Extraction of individual tree attributes using ultra-high-density point clouds acquired by low-cost UAV-LiDAR in Eucalyptus plantations

Mei Zhou[1], Chungan Li[2*] and Zhen Li[3]

Abstract

Key message In this paper, we first introduced a novel method for directly measuring tree diameters from UAV-LiDAR point clouds utilizing the χ^2-filtering technique and a technique for measuring tree heights using pseudo-waveforms.

Context Eucalyptus plantation forests constitute the largest expanse of planted broad-leaved forests worldwide. Detailed and accurate individual tree attributes are essential for precision forestry. Terrestrial laser scanning (TLS) and mobile laser scanning (MLS) are frequently employed to acquire information on individual trees. However, both technologies suffer from low efficiency. Therefore, the challenge remains how to access this information efficiently.

Aims Consequently, this paper investigated a novel technical approach to automatically extract individual tree attributes using low-cost UAV-LiDAR technology.

Methods The framework consists of three independent yet interrelated approaches. Firstly, the tree trunks were detected using an approach based on the hierarchical density-based spatial clustering of applications with noise (HDBSCAN) algorithm. It utilized 3D point clouds to achieve precise tree counts and their approximate locations. These locations then enabled cylindrical segmentation of the point clouds at the trunk level, facilitating diameter measurement. Secondly, stem diameters were directly measured using the probability density function of the chi-square distribution. This process produced precise stem diameters, trunk positions, and growth directions, which were subsequently used to determine the center of the crown top for tree height extraction. Lastly, the tree height was estimated based on the pseudo-waveforms. We validated this framework by acquiring ultra-high-density UAV-LiDAR data in an Eucalyptus plantation.

Results The result indicated a precision of 91.1% for individual tree detection, with an *F*-score of 0.916. The root mean square errors (RMSEs) for direct measurements of diameter at breast height (DBH) and tree height were 14.60% (2.18 cm) and 2.69% (0.31 m), respectively. Furthermore, this study suggested that the classical circle-fitting method might not be suitable for directly measuring tree diameter using low-cost UAV-LiDAR data.

Conclusion The proposed framework facilitates automated inventory and monitoring in Eucalyptus plantation forests. However, more trials are needed to verify the framework's applicability in other planted and natural forests.

Handling editor: Shengli Tao.

*Correspondence:
Chungan Li
chungan@gxu.edu.cn
Full list of author information is available at the end of the article

Keywords Individual tree detection, Tree count and position, Stem diameter, Tree height, Chi-square distribution, Pseudo-waveforms

1 Introduction

Since the beginning of the century, airborne LiDAR technology has emerged as a practical tool for forest inventories at various scales, from forest stands to local to national levels (Næsset et al. 2004; Maltamo and Packalen 2014; White et al. 2017; Li et al. 2023). Regional airborne LiDAR forest inventories typically adopt the area-based approach (ABA). This two-stage procedure comprehensively maps forest attributes, such as mean diameter at breast height (DBH), mean height, basal area, stand volume, and above-ground biomass (Næsset and Bjerknes 2001; Næsset 2002). Since the pioneering application in 2010 (Jaakkola et al. 2010), UAV-LiDAR has rapidly gained popularity as an appealing alternative to airborne LiDAR due to its ease of deployment, flexible sensor configurations, high temporal and spatial resolution, adaptable and reproducible data acquisition, and cost-efficiency (Kukkonen et al. 2022). As a result, UAV-LiDAR is widely employed for local-scale forest management inventory and monitoring (Dainelli et al. 2021). Its low altitude and slow flight speed enable UAV-LiDAR to generate high-density point clouds, effectively penetrating the forest canopy and capturing comprehensive information across the vertical profile. Consequently, this improves the accuracy of estimating structural forest attributes (Dalla Corte et al. 2020). Besides utilizing the conventional ABA for forest attribute estimation (López-Amoedo et al. 2023; Maesano et al. 2022; d'Oliveira et al. 2020), UAV-LiDAR also facilitates precise extraction of forest tree specifics, encompassing tree count, location, and attributes. These attributes are achieved through individual tree segmentation (ITS) techniques, allowing for the accurate measurements of diameter, tree height, crown-based height, crown area, canopy volume, stem volume, and biomass (Zhang et al. 2022a; Krůček et al. 2020). Furthermore, UAV-LiDAR can derive the stand volume and biomass by utilizing estimated taper curves (Liang et al. 2019; Hyyppä et al. 2020b) or allometric equations (Lin et al. 2023), therefore replacing the field plot measurements in regional airborne LiDAR applications (Xiang et al. 2024). UAV-LiDAR also offers additional capabilities, such as reconstructing tree branching structures (Cárdenas et al. 2022), determining growth direction (Neuville et al. 2021), and aiding in the classification of forest types and species (Scheeres et al. 2023; McGaughey et al. 2024; Hakula et al. 2023). The ABA primarily captures a group of mean forest attributes within a grid. However, the individual tree approach provides detailed information about trees, which is crucial for understanding the forest ecosystem structure and function comprehensively and precisely (Guo et al. 2020). This information also benefits precision forestry management (Fu et al. 2024).

This paper primarily focuses on extracting individual tree attributes using low-cost UAV-LiDAR technology in Eucalyptus plantation forests. These forests represent the vastest expanse of planted broad-leaved forests worldwide, with eucalyptus trees being cultivated in over 100 countries across six continents, covering an area exceeding 20 million hectares (Hua et al. 2022; Zheng and Wang 2021). As such, investigating the automatic acquisition of parameters related to eucalyptus plantation forests is immensely importance for precision forestry. The low-cost UAV-LiDAR system is comparable to the survey-grade UAV-LiDAR system, exemplified by the Riegl VUX- 1 laser scanner (Riegl Laser Measurement System GmbH, Horm, Austria), which is characterized by its range-accuracy of 1 cm (Li et al. 2019; Kuželka et al. 2020). Although the range accuracy of low-cost UAV-LiDAR systems is not as high as survey-grade UAV-LiDAR systems, they are less expensive, making them widely affordable in practical forest management applications. This study includes three key facets: determining the tree count and their locations and measuring their diameters and heights. Determining tree count and position relies on individual tree detection (ITD), also called ITS (Pu et al. 2023). Numerous studies have been focused on ITD or ITS, resulting in numerous detection methods. These methods are further classified into two groups: individual tree crown (ITC) detection, which segments trees by identifying gaps between neighboring crowns (Deng et al. 2024), and trunk detection, which emphasizes the isolation of tree trunks. Tree crown detection techniques can be further classified into raster-based and point cloud-based approaches (Soininen et al. 2022). Classical algorithms include the watershed and its variants, graph-cut segmentation (Strîmbu and Strîmbu 2015), and fishing net dragging simulations (Liu et al. 2015). Although raster-based methods have advantages in computational efficiency and detection of dominant trees, they lose 3D information during rasterization and may miss smaller trees beneath the canopy (Jeronimo et al. 2018). In contrast, point cloud-based methods directly segment individual trees from voxel or point cloud spaces (Deng et al. 2024), assuming that the canopy center exhibits a higher point cloud density (Mongus and Žalik 2015). Segmentation techniques are mainly clustering algorithms, such as region growing (Li et al. 2012; Torresan et al. 2020), layer-stacking (Ayrey et al. 2017), K-means (Gupta et al. 2010), mean-shift (Xiao et al. 2019), normalized cut (Yan et al. 2018), and density-based spatial clustering of applications with noise (DBSCAN) (Neuville et al. 2021). Deep learning networks have recently gained much attention in ITS. These algorithms include YOLO (Sun et al. 2022; Straker et al. 2023), ForAINet (Xiang et al. 2024), and PointNet + + (Kim et al. 2023). Although point cloud-based segmentation demands much computational resources, it often achieves higher accuracy. However, it is easy to produce omissions and commission errors when the crowns are squeezed against each other and the shape of the crowns is irregular. Trunk detection also utilizes 3D point clouds to detect individual trees. However, it focuses only on a specific height interval (the trunk layers). The significant algorithms currently in use include DBSCAN, random sample consistency (RANSAC) (Deng et al. 2024), Hough transform, robust least trimmed squares (RLTS), supervised individual-tree squares (RLTS) (Kuželka et al. 2020), and graph-cut clustering (Williams et al. 2020; Dersch et al. 2021). Due to the distinct clustering of point clouds, trunk detection tends to be more accurate. However, it needs a high point cloud density. To improve detection accuracy and computational effectiveness, we need to improve existing algorithms and develop new ones adapted for various forest scenarios, especially for complex ones, such as natural forests and planted forests with rich understory vegetation.

DBH and height are the critical individual tree attributes. The primary method for direct measurements of individual tree DBH using UAV-LiDAR data relied on a circle-fitting algorithm grounded in the geometry of the point cloud distribution. This approach involved fitting the circles or cylinders of LiDAR point clouds at horizontal trunk sections (“slices” or “bins”), such as cylinders encompassing trunk heights of 1.2–1.4 m (Brede et al. 2017), as described by Kukkonen et al. (2022). For a long time, the circle-fitting technique for measuring tree diameters has been implemented in terrestrial laser scanning (TLS) (Maas et al. 2008). TLS has a high density, high positional accuracy of point clouds, and a near-circular or arc-shaped distribution of laser points on the trunk (Liu et al. 2018). Therefore, its direct measurement of diameters is usually very accurate (Lee and Lee 2024). For UAV-LiDAR, especially for low-cost LiDAR, direct diameter measurement is difficult to achieve the desired accuracy due to the sparse point clouds of tree trunks (Neuville et al. 2021) and limited precision in point cloud positioning (Lin et al. 2021). Although some studies employed principal component analysis (PCA) for directly measuring tree diameters, their results were slightly worse than those of the circle-fitting methods (Jaakkola et al. 2017). Therefore, we must explore innovative algorithms to enhance the accuracy of directly measuring diameters. Analyzing the probability distribution of the point clouds surrounding the trunk might help us develop new diameter measurement methods. On the other hand, direct UAV-LiDAR measurements of tree height are both straightforward and precise. The primary method entails calculating tree height by measuring the distance from the topmost point of the crown to the ground, which is accomplished through the techniques of individual tree detection and segmentation. Both CHM (Lin et al. 2021; Picos et al. 2020; Ganz et al. 2019) and 3D point clouds (Dalla Corte et al. 2020; Krůček et al. 2020; Hyyppä et al. 2020b) could be utilized for extracting tree height. However, maintaining consistency between the tree heights extracted by CHM or 3Dpoint clouds and those obtained through field measurements remains a significant challenge. Despite the exceptional data quality of survey-grade UAV-LiDAR, its high cost (Hu et al. 2021) often exceeds its practicality for forest resource applications (Wallace et al. 2012). Therefore, exploring the utilization of low-cost UAV-LiDAR data to extract individual tree attributes for “automated forest inventory” (Xiang et al. 2024) or “autonomous forest field investigation” (Jaakkola et al. 2017) remains a critical research focus in the academic community.

The primary goal of this paper was to automatically extract individual tree attributes, encompassing tree count and position, stem diameter, and height, using low-cost UAV-LiDAR technology. To fulfill this goal, UAV-LiDAR and ground-truth data were collected in an Eucalyptus plantation. The specific objectives encompassed: (1) developing a methodology to determine the number and location of forest trees using 3D point clouds based on the HBDSCAN algorithm; (2) examining the statistical distribution of point clouds on the trunks and proposing an innovative approach for directly measuring stem diameter using 3D point clouds based on the probability density function (PDF) of the chi-square (χ^2) distribution; and (3) introducing a pseudo-waveform-based approach to extract tree height, yielding estimates that align closely with field measurements. The authors hope to offer a novel framework for automated forest inventory and monitoring in forest plantations.

2 Materials and methods

2.1 Test site

The study area encompasses an intensively managed *Eucalyptus urophylla* S. T. Blake plantation, spanning 0.4 hectares and located within the state-operated Gaofeng forest farm (Zhang et al. 2019) in the center of the Guangxi Zhuang Autonomous Region, southern China (108°35′27″E, 22°59′59″N) (Fig. 1a, b, and c). This forest is seven years old and is a second-rotation coppice of fast-growing Eucalyptus plantations, established after the original forest underwent clear-cutting in the spring of 2015, with a 6–8-year rotation cycle. The initial planting adhered to contour lines, maintaining a spacing of approximately 2 × 3 m (1667 trees·ha^{-1}). Significantly, all trees within this forest were of the same age and exhibited uniform growth in diameter and height (Fig. 1d). The terrain of the study area is characterized by hilly and mountainous landscapes, with altitudes ranging from 174.6 to 234.3 m above sea level. Slopes range from 15° to 35°, with an average slope of 25°. The forest was abundant in understory trees, herbaceous plants, climbing vines, and stripped but not yet shed bark.

2.2 Data collection

On April 8, 2022, the LiDAR data acquisition mission was conducted using the DJI Matrice 300 RTK UAV system from Shenzhen Dajiang Innovation Technology Co. Ltd. (Shenzhen, China). The 6.3 kg quadcopter UAV system is equipped with an Automatic Dependent Surveillance-Broadcast (ADS-B) anti-collision system, enabling it to achieve a positioning accuracy of 1.0–1.5 cm +1 ppm through the real-time kinematic-global navigation satellite system (RTK-GNSS). The M300 RTK can be equipped with various sensors, including the DJI Zenmuse P1 camera and the DJI Zenmuse L1 laser scanner for aerial surveys. The Zenmuse L1 integrates Livox LiDAR modules, a high-precision IMU, and a 50-megapixel CMOS camera on a three-axis stabilized gimbal. It boasts a range of 450 m with a field of view (FOV) of 70° and can manage up to three echoes per laser emission. In the repetitive scanning mode, the L1 sensor achieves a point rate of up to 480,000 points per second. The system attitude accuracy is 10 cm, while the altitude accuracy is 5 cm at a flight altitude 50 m above the ground. The laser scanner's distance measurement accuracy (RMS1σ) is 3 cm @ 100 m.

During the data acquisition phase, the flight mode was set to terrain-following, with a flight altitude maintained 50 m above the ground surface. The flight speed was set at 5 m·s^{-1}, and a strip overlap rate of 60% was employed to ensure data redundancy. Mutually perpendicular directions were used for repeated scanning to achieve

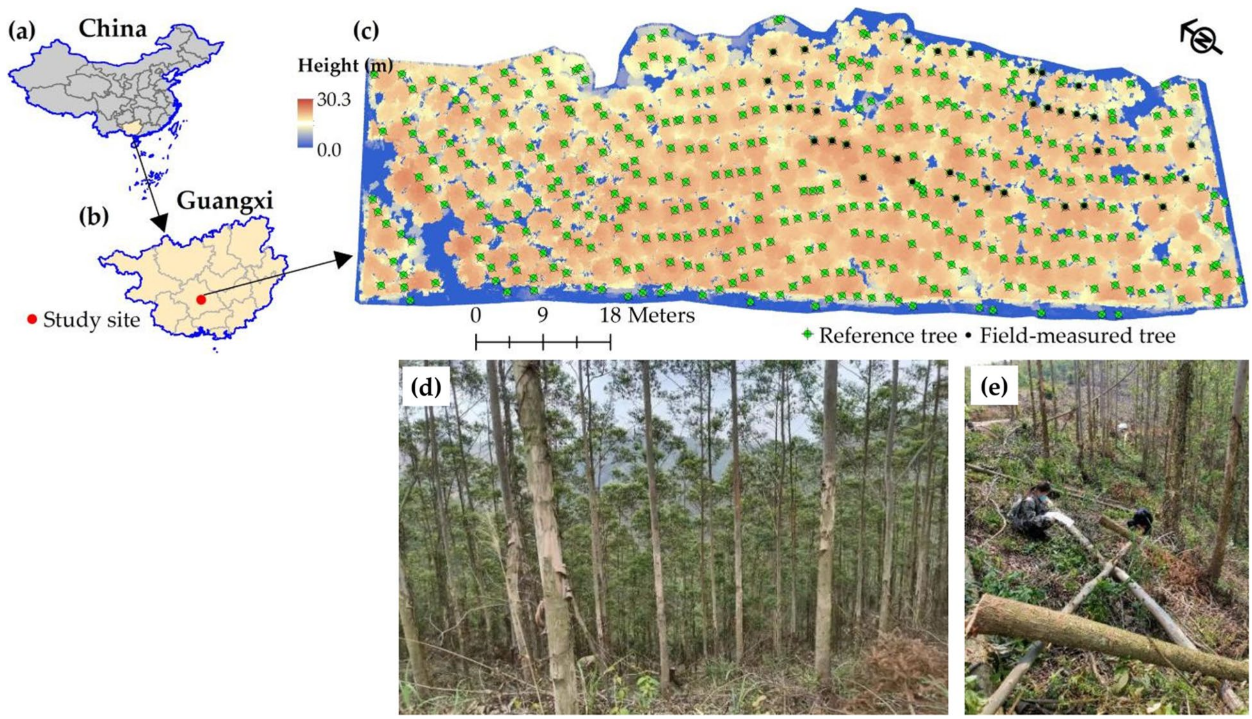

Fig. 1 Study site and forest stands. (**a**) Location of Guangxi in China; (**b**) location of study site in Guangxi; (**c**) CHM of the study site and the location of the reference trees and the field-measure tree; (**d**) forest stand just before logging; and (**e**) the measurements of the felling tree at the time of logging down

ultra-high-density point cloud data. The collected laser point cloud data was preprocessed using TerraSolid software (Terrasolid, Helsinki, Finland). This preprocessing included point cloud classification using the progressive triangular irregular network (TIN) filtering algorithm, and digital elevation model (DEM) production. The DEM (0.5 m resolution) was then utilized to normalize the laser point cloud elevation. The final mean point cloud density achieved was 19,230 pts·m^{-2}. The point cloud density was further analyzed based on altitude ranges, revealing 982 pts·m^{-2} below 1 m, 4388 pts·m^{-2} between 1 and 6 m, and 13,861 pts·m^{-2} above 6 m.

There were 413 trees in the study site. On April 10, 2022, the DBHs (1.3 m above ground) of the 33 trees with DBH ≥ 5 cm were measured using a steel tape, and the stem coordinates were obtained using the network RTK-GNSS of Hi-Target D8pro (Hi-Target Satellite Navigation Technology Co. Ltd. Guangzhou, China) based on the Qianxun continuously operating reference station (CORS) network, with a horizontal positioning accuracy of ± 8 mm. Two days later, as the forests were cleared cut, the diameters of the felled reference trees at 2, 4, 6 m, ... were measured one by one, and their total lengths (heights) were measured using a tape measure on the trunk (Fig. 1e). The individual stem volume (VOL) was calculated using the following allometric equation (Zhang et al. 2022b).

$$VOL = 4.354 \times 10^{-5} DBH^{1.71874} H^{1.1927} \quad (1)$$

where DBH is the diameter at breast height, H is the tree height. The mean DBH, height, and stem volume of the 33 field-measured reference trees were 15.19 ± 2.10 cm, 19.75 ± 1.46 m, and 0.1708 ± 0.0479 m^3, respectively.

2.3 Methodology for extracting individual tree attributes

The procedure for extracting individual tree attributes using ultra-high-density point clouds comprised three distinct yet interrelated steps:

- Determination of tree count and stem location. The first step involved identifying the number of trees within the stand and locating the center of the stem base. This step was achieved through trunk detection based on the HDBSCAN algorithm (Neuville et al. 2021), enabling the calculation of the total tree count and the approximate coordinates of the stem centers at 2 m above ground level.
- DBH measurement. This step involved cylindrical clipping point clouds of the trunk, directly measuring tree diameters, and extracting the precise coordinates of the trunk's center by filtering point clouds using the PDF of χ^2 -distribution. This step also obtained the DBH and its center position, the diameter, and center position at a tree height of 7 m.
- Estimation of tree height. The final step involved calculating the center of the crown top based on the coordinates of the stem centers at heights of 1.3 m and 7.0 m and the canopy height model (CHM). With the cylindrical segmentation of the crown's point clouds, this step finally extracted the tree height based on pseudo-waveforms.

The entire procedure of individual tree attribute extraction is illustrated in Fig. 2.

In this paper, individual tree attributes were extracted fully automatically, without manual intervention. All codes for the process were written in Python (Python Software Foundation, Python version 3.8).

2.3.1 Tree stem detection

Identifying trees' quantity and approximate locations is pivotal in extracting individual tree attributes. Our study employed the HDBSCAN algorithm for trunk detection, aiming to determine the tree count and their positions. The methodology entails the following steps:

(1) Segmentation of point clouds of the trunk layer. The understory canopy and tree foliage exert a significant impact on trunk detection. After repeated trials, the normalized point clouds with 2–4 m height were cropped and utilized for trunk detection to minimize these effects.
(2) HDBSCAN clustering. The HDBSCAN algorithm was used to cluster the point clouds of four height slices, i.e. 2–2.5 m, 2.5–3 m, 3–3.5 m, and 3.5–4 m, at the trunk layer to obtain clusters of the point clouds, respectively. Labels were then assigned to each cluster, denoted as $C_i^h (h = 1, 2, \cdots, 4;\ i = 1, 2, \cdots, n)$, where h is the number of height slices, and n is the total number of clusters. The results of this clustering for trunk detection were of utmost importance.
(3) Noise filtering and trunk diameter extraction. For the point clouds of each cluster, the PDF of χ^2 -distribution was employed to effectively filter out noises and calculate the approximate diameter (D_i^h, $h = 1, 2, \cdots, 4$, $i = 1, 2, \cdots, n$) of the tree trunk and its geometric central coordinates (x_{0i}^h, y_{0i}^h) for each height slice. The detailed methodologies for these processes are outlined in Sect. 2.3.2.
(4) Cluster matching. If the point cloud density is high enough, there will always be a large number of continuously distributed point clouds in the vertical direction of the tree stem. Consequently, the trunk center coordinates (x_i^1, y_i^1) of the cluster within first height slice were utilized as a reference to systemati-

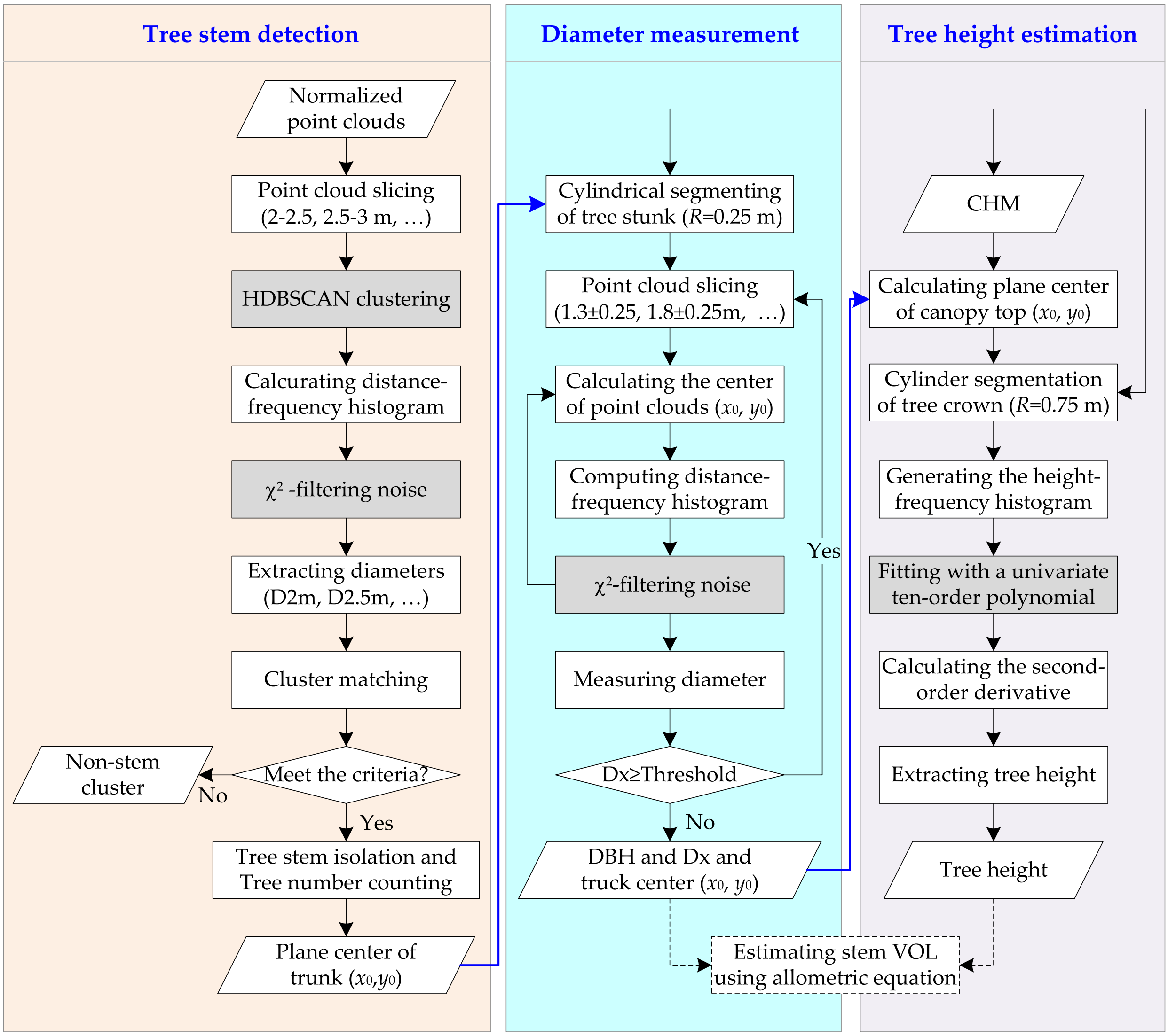

Fig. 2 A flowchart depicting the procedures for extracting individual tree attributes using UAV-LiDAR data. Dx: diameters at height-intervals of 2–2.5 m, 2.5–3 m, or 1.3 ±0.25 m, 2.0 ±0.25 m, 3.0 ±0.25 m, etc

cally assign each cluster of the remaining height slices according to the following criteria: For the i cluster of the first height slice, if the distance ($d(1i, kj)$) between the center horizontal-plane coordinates (x_j^k, y_j^k) of the j cluster of the k height slice and (x_i^1, y_i^1) was less than 50 cm (depending on the lean of the stem and the structure of understory vegetation, e.g., the more understory vegetation, the greater the distance), i.e. $d(1i, kj) = \sqrt{(x_i^1 - x_j^k)^2 + (y_i^1 - y_j^k)^2} \leq 50$ cm, it was concluded that cluster C_j^k belongs to the same trunk as cluster C_i^1. Once all clusters across all height slices had been analyzed, all point cloud clusters could be matched, indicating the completion of trunk isolation. Clusters absent in the first height slice but present in others were deemed non-stem clusters and excluded from further steps.

(5) Tree stem determination and isolation. For a given trunk, if two of the four height slices had a diameter greater than 5 cm and less than 35 cm (depending on the lean of the stem and the structure of understory vegetation), the trunk was determined to be a tree stem. Otherwise, the trunk was not a tree stem but might be the canopy of undergrowth vegetation or a climbing vine.

(6) Determination of the approximate horizontal-plane center of tree stem. For the cluster belonging to the tree stem, the remaining point clouds after filtering by the PDF ofχ^2 -distribution in the first height slice

was used to calculate the approximate horizontal-plane center of the tree stem $(x_0^{1,i}, y_0^{1,i})$.

2.3.2 Direct measurement of tree diameters

A buffer zone, whose radius is 0.25 m but may vary based on factors such as the diameter distribution of trees and the density of understory vegetation (for instance, a denser understory may necessitate a smaller radius), was delineated around the base horizontal-plane center of the tree, as determined in Sect. 2.3.1. This buffer zone was then utilized to perform a cylindrical clipping of the tree trunk's point clouds. When extracting a tree trunk's diameter at a specific height, a ± 0.25-m (depending on the point cloud density, the higher the point cloud density; the smaller the height interval) point cloud segment centered on that height was clipped. Figure 3a illustrates the point cloud clipping for DBH extraction.

The inertial measurement unit (IMU), global navigation satellite system (GNSS), and laser sensors employed in this study were of non-survey-grade quality, resulting in less-than-optimal spatial positional accuracy with horizontal positional errors approximately measuring 10 cm (Stroner et al. 2023). Consequently, the distribution of laser point clouds within the trunk cross-section displayed a nearly solid circular pattern accompanied by overlap (Fig. 3b). We calculated the horizontal plane center of the point clouds inside the cylinder and the distance of each point cloud from that center. Following this, we segmented the distance from the trunk's center to the outermost point cloud (representing the maximum distance) into 50 equal intervals (depending on the number of point clouds in the tree trunk, the larger the number of point clouds, the larger the number of distance intervals). We then computed the frequency of the point clouds within each interval to produce a distance-frequency histogram illustrating the point cloud distribution, as shown in Fig. 3c.

Since tree trunks do not allow for penetration of laser point clouds, their position errors were random. It is assumed that the trunk's point clouds follow a normal distribution centered on the bark. When the trunk's radius exceeds the point cloud's error, we postulate that the laser plus hitting and echoing from the trunk in a particular direction obeys a normal distribution centered on the bark. Furthermore, we hypothesize that the distance-frequency histogram of the point clouds (Fig. 3c) follows a χ^2 -distribution with ν degrees of freedom, denoted as $X \sim {}^2(\nu)$. Consequently, in this study, the PDF of χ^2 -distribution was employed to model the distance-frequency histogram of the trunk's point clouds, and the trunk diameter was determined after eliminating all anomalous data at a threshold of $\alpha = 0.05$. The direct measurement of tree diameters was conducted on a per-tree basis. The methodological steps for the direct measurement of DBH are described in detail below. This procedure also measures diameters at other heights (e.g., 1.8 m, 2.0 m, 3 m).

(1) Cylindrical segmenting point clouds on the trunk. Firstly, a buffer zone with a radius of 0.50 m was generated based on the center of the tree trunk obtained in Sect. 2.3.1. Then, a cylinder with a radius of 0.5 m and a height of 0.5 m (1.3 m ± 0.25 m) was utilized to segment the point clouds at 1.3 m of

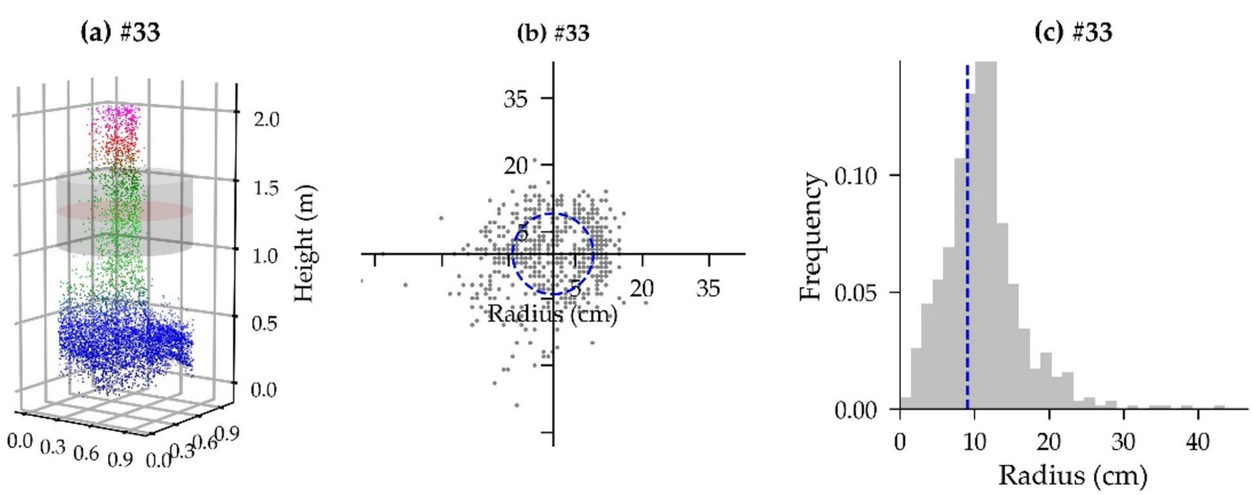

Fig. 3 3D trunk's point clouds and their distribution. Cylindrical segmentation of the trunk's point clouds (**a**). Their distribution in the trunk's cross-section (**b**). Their 2D distance-frequency histograms (**c**). The blue dashed circles and vertical lines in (**b**) and (**c**) are the simulated positions of the trunk and bark based on field-measurements, respectively

trunk height (Fig. 3a). These point clouds were used to measure the DBH of the trees.

(2) Calculating the coordinates (x_0, y_0) of the plane geometry center of the point clouds on the trunk: $x_0 = \frac{1}{N}\sum_{i=1}^{N} x_i$, $y_0 = \frac{1}{N}\sum_{i=1}^{N} y_i$, where x_i and y_i is the horizontal-plane coordinates of point clouds, N is the total number of point clouds.

(3) Calculating the distances $(d(i))$ between point clouds and the geometric center of the trunk: $d(i) = \sqrt{(x_i - x_0)^2 + (y_i - y_0)^2}$, and their maximum distance is $d_{\max}$, $d_{\max} = \max_{i \in N}(d(i))$.

(4) Calculating the distance-frequency histogram. The interval $[0, d_{\max}]$ was divided into 50 uniform intervals, and the relative frequency $(f(d_i))$ of the point clouds of each interval was calculated by the ratio of the point clouds present in a specific interval to the total number of point clouds. Specifically, $f(d_i) = n(d_i)/N$ represents the relative frequency, where $n(d_i)$ is the count of point clouds within the i distance interval, N is the total number of point clouds. Based on these calculations, a distance-frequency histogram was generated (Fig. 3c).

(5) Noise filtering. The distance-frequency histogram was fitted using the χ^2 -distribution, resulting in a PDF, $f(x)$, which was given by $f(x) = \begin{cases} \frac{1}{2^{\nu/2}\Gamma(\nu/2)} x^{\frac{\nu}{2}-1} e^{-x/2}, x > 0 \\ 0, x \leq 0 \end{cases}$, where x is the distance, ν is the degree of freedom, and Γ is the gamma function. To remove anomalous data (noise), a threshold of $\alpha = 0.05$ was employed.

(6) Repeated steps (2)–(5) until no anomalous data were removed.

(7) Extraction of trunk diameter. After thoroughly removing all anomalous data, the distance associated with the peak probability density value was defined as the radius (R) of tree trunk, e.g., $R = x$, $x \in \max f(x)$. Subsequently, the DBH was yielded, calculated as $DBH = 2R$.

In extracting tree diameters, abnormal diameter estimates (too large or too small) often arose due to the influence of branch, understory and herbaceous canopies, climbing vines, and barks that have been stripped but has not yet shed (this is common in eucalyptus forests). Based on statistics from 192 field plots of Eucalyptus forests with an average height of at least 15.0 m in Guangxi, it was found that only 3.5% of the trees had a diameter of 20 cm or more (Zhang et al. 2022b). Therefore, the subsequent rule for determining the tree trunk diameter was formulated as follows:

(1) The threshold for individual tree diameter was established between 5 and 20 cm. If the initially measured diameter fell outside this range, we moved 0.5 m upward from the designated trunk height (for example, we moved up from 1.3 m to 1.8 m), re-segmented the point clouds, and measured the diameter again. If the newly acquired diameter fell within the diameter threshold range, it should supersede the previous measurement. On the contrary, if the new diameter remained outside the diameter threshold range, it descended 0.5 m from the original trunk height (for example, moved down from 1.3 m to 0.8 m), re-segmented the point clouds, and conducted another diameter measurement.

(2) Repeat the procedure of upward-downward movement, maintaining a height interval of 0.5 m for each movement, to re-segment the point clouds and re-extract the tree diameters. If none of the tree diameters within the range of specified height ±1.0 m (example: 1.3–1.0–1.3 +1.0 m.) fell within the diameter threshold range, the tree diameter was replaced by the average diameter of all the trees.

Utilizing point clouds without noises, we computed the geometric centers, $(x_0^{1.3}, y_0^{1.3})$ and (x_0^{7}, y_0^{7}), for the cross-sections at stem heights of 1.3 m and 7.0 m, respectively. These centers determined the tree's growth direction and the crown's apex (shown in Sect. 2.3.3). Although we could derive the centers of trunks of different heights, we chose to use $(x_0^{1.3}, y_0^{1.3})$ as the trunk's centroid in this study to align with methodologies employed in other research. Owing to the impact of the understory vegetation, a small number of trees might exist wherein all measured trunk diameters exceeded the maximum diameter threshold within the specific height intervals of 0.8–2.3 m and 6.0–8.0 m. For these particular trees, we utilized noise-filtered point clouds, aligning with their most minor diameter, to determine the geometric centers of the trunks at the heights of 1.3 m and 7.0 m.

In addition to extracting tree diameters using the methods above, we employed a classic circle-fitting method to extract the DBH to evaluate its suitability for directly measuring tree diameter using low-cost UAV-LiDAR point clouds.

2.3.3 Tree height and stem volume estimations

Pinpointing the crown top is crucial to measuring tree heights accurately. Since Eucalyptus trees have tall, slender stems that are often slightly angled rather than perfectly perpendicular to the ground, especially those located at the edge of the stand (Fig. 1d and e), the task becomes more challenging. Based on the stem centers measured at heights of 1.3 m and 7.0 m, along with the CHM, we calculated the plane coordinates of the crown's apex. Following this, the crown was segmented. We utilized pseudo-waveforms (Muss et al. 2011) to estimate tree heights, minimize the impact of elevated objects like birds or sporadically distributed point clouds hovering above the canopy, and be consistent with field measurements. The extraction of individual tree heights involved several steps, as outlined below:

(1) Calculating the plane coordinates of the canopy top. The planar coordinates of the canopy top were calculated by the following methods and steps.

- For tree $\overrightarrow{oA}$, according to Sect. 2.3.2, the coordinates of the center of its stem at 1.3 m (a) and 7.0 m (b) in 3D space are $(x_{1.3}, y_{1.3}, z_{1.3})$ and (x_7, y_7, z_7), where: $z_{1.3} = 1.3$, $z_7 = 7$ (Fig. 4). The coordinate origin point o is at the tree's base, which central coordinates at (x_0, y_0, z_0), where: $x_0 = x_{1.3} + (x_7 - x_{1.3}) \times \frac{5.7}{1.3}$, $y_0 = y_{1.3} + (y_7 - y_{1.3}) \times \frac{5.7}{1.3}$, $z_0 = 0$.
- Let $\vec{oA}$ projects onto the xoy plane as $\overrightarrow{oB}$, and the angle between $\overrightarrow{oB}$ and the xoy plane is β, then,

$$\beta = \arccos\left(\frac{x_7 - x_{1.3}}{\sqrt{(x_7 - x_{1.3})^2 + (y_7 - y_{1.3})^2}}\right) \tag{2}$$

- Let α be the angle in plane zoB, then,
- Suppose in CHM, the projection of $\overrightarrow{oA}$ is $\overrightarrow{o'A}$. The coordinate of any pixel c in the direction of $\overrightarrow{o'A}$ (determined by β) are (x_c, y_c, z_c). Suppose the angle $\angle coB$ in the zoB plane is λ, then,
- A is the center at the top of the tree crown, and its coordinate was $(x_{top}, y_{top}, z_{top})$. When λ= α, c coincides with point A, meaning c is the vertex of the tree crown at $\overrightarrow{oA}$. At this point, the z-value of pixel c, z_{top}, can be read from CHM. Therefore, the coordinates of A in the xoy plane are:

(2) Let $\overrightarrow{oA}$ projects onto the xoy plane as $\overrightarrow{oB}$, and the angle between $\overrightarrow{oB}$ and the xoy plane is β, then,

$$\beta = \arccos\left(\frac{x_7 - x_{1.3}}{\sqrt{(x_7 - x_{1.3})^2 + (y_7 - y_{1.3})^2}}\right) \tag{3}$$

Let α be the angle in plane zoB, then,

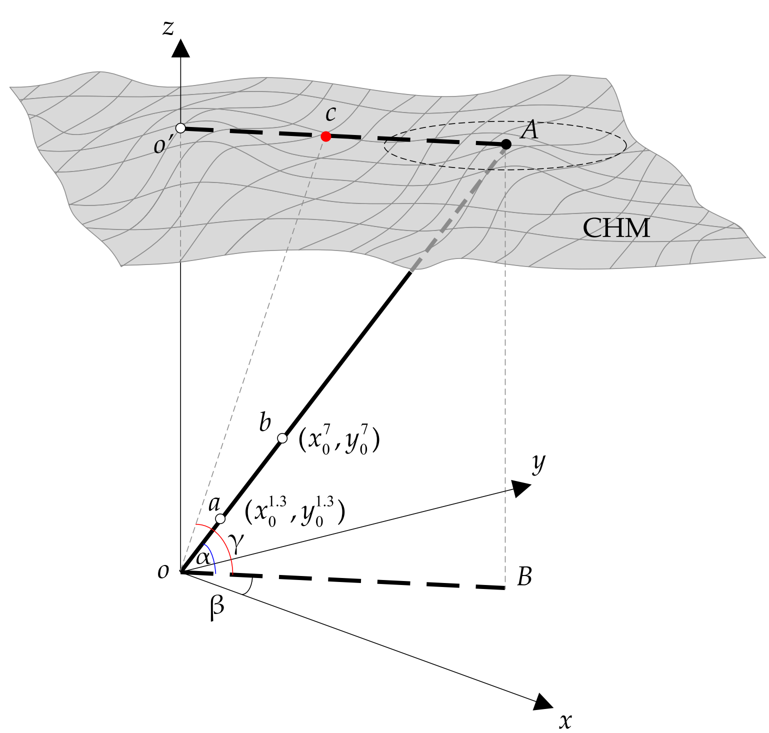

Fig. 4 Calculating the coordinates of the center of the crown top based on the coordinates of the tree stem at heights of 1.3 m and 7.0 m and CHM. The black dotted ellipse centered on *A* illustrates the extent of crown segmentation (radius of 0.75 m)

$$\lambda = \arccos\left(\frac{(x_c - x_{1.3})(x_7 - x_{1.3}) + (y_c - y_{1.3})(y_7 - y_{1.3})}{\sqrt{(x_c - x_{1.3})^2 + (y_c - y_{1.3})^2 + (z_c - z_{1.3})^2} \times \sqrt{(x_7 - x_{1.3})^2 + (y_7 - y_{1.3})^2}}\right) \quad (4)$$

Suppose in CHM, the projection of $\overrightarrow{oA}$ is $\overrightarrow{o'A}$. The coordinate of any pixel c in the direction of $\overrightarrow{o'A}$ (determined by β) are (x_c, y_c, z_c). Suppose the angle $\angle coB$ in the zoB plane is λ, then,

$$x_{top} = x_{1.3} + \frac{(z_{top} - z_{1.3})(x_7 - x_{1.3})}{z_{top} - z_{1.3}}, \; y_{top} = y_{1.3} + \frac{(z_{top} - z_{1.3})(y_7 - y_{1.3})}{z_{top} - z_{1.3}} \quad (5)$$

A is the center at the top of the tree crown, and its coordinate was $(x_{top}, y_{top}, z_{top})$. When λ = α, c coincides with point A, meaning c is the vertex of the tree crown at $\overrightarrow{oA}$. At this point, the z-value of pixel c, z_{top}, can be read from CHM. Therefore, the coordinates of A in the xoy plane are:
$x_{top} = x_{1.3} + \frac{(z_{top}-z_{1.3})(x_7-x_{1.3})}{z_{top}-z_{1.3}}$,
$y_{top} = y_{1.3} + \frac{(z_{top}-z_{1.3})(y_7-y_{1.3})}{z_{top}-z_{1.3}}$ (5).

(2) Cylinder segmentation of the tree crown. A buffer zone with a radius of 0.75 m (depending on the size of the crown diameter and the density of the tree, e.g., the greater the density of trees, the smaller the radius.) was generated at the center of the crown top (x_{top}, y_{top}) for cylindrical segmentation of the individual tree crown to extract the point clouds of the crown (Fig. 5a, c).

(3) Calculating the height-relative frequency histogram. The point cloud data was divided into 100 height bins, spanning from the highest point to the ground. The height of each bin is $\frac{h\max}{100}$. Subsequently, the frequency of the point clouds within each height bin was calculated (also referred to as the fractional cover, representing the proportion of all point clouds contained in that bin). This process resulted in the generation of height-relative frequency histograms for the point clouds (Fig. 5b, d).

(4) Fitting the height-relative frequency histograms. A univariate ten-order polynomial, $f(x) = \sum_{i=1}^{10} a_{i-1}x^{10-i+1} + k$, where $f(x)$ is the point cloud frequency, x is the median height of the height bins, $a_i (i = 1, 2, \cdots, 10)$ is the model coefficient, k is the constant, was used to fit the height-frequency histogram using the least-squares method to obtain the pseudo-waveform of the height-frequency histograms (Fig. 5b, d). $f(x)$ is continuous in the interval $[0 + \frac{1}{2} \times \frac{h\max}{100}, h\max - \frac{1}{2} \times \frac{h\max}{100}]$.

(5) Identifying the convex and concave intervals. Calculate the second-order derivative $f''(x)$ of $f(x)$. Find all inflection points for $f''(x) = 0$ and add two inflection points for $x = 0$ and $x = h\max$. Divide the $f(x)$ into intervals based on the inflection points. If in the interval [a, b], $f''(x) > 0$, $f(x)$ is concave and the interval is concave; if in the inter-

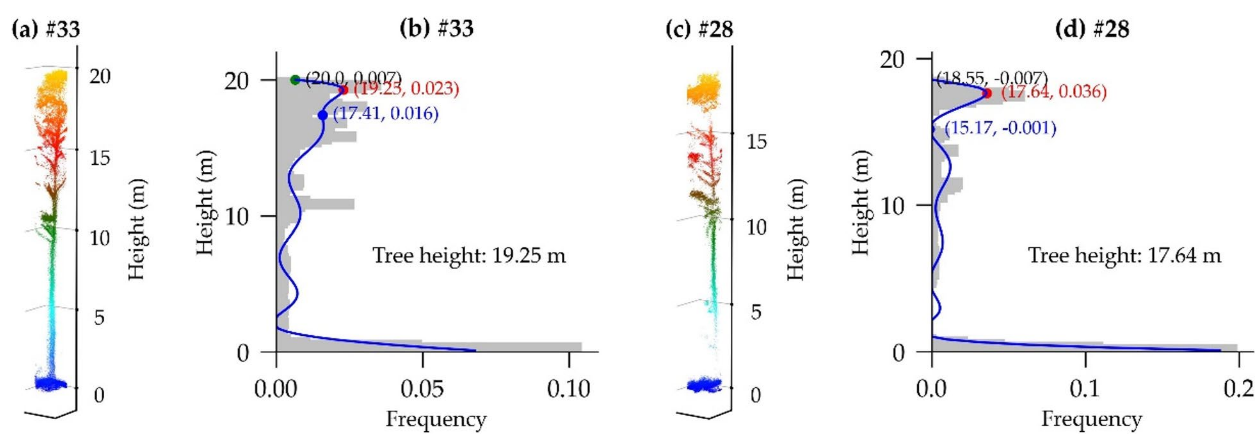

Fig. 5 Extraction of individual tree heights via pseudo-waveforms. (**a**) and (**c**) are 3D point clouds of individual tree crowns clipped from cylinders, (**a**) is an upright tree, and (**c**) is an inclined tree. (**b**) and (**d**) are histograms of the height-frequency (coverage) of the point clouds and pseudo-waveform fitted by an univariate ten-order polynomial, with the red dots being the extreme points of the highest convex intervals, the height of which is the tree height

val $[c, d]$, $f''(x) < 0$, $f(x)$ is convex and the interval is convex. Using this method, we can divide $f(x)$ into a number of convex and concave intervals.

(6) Finding the extreme points. In the concave interval $[a, b]$, if $A = \min f(x)$, $x \in [a, b]$, A is a minimum, and (A, x) is a minima point; in the convex interval $[c, d]$, if $A = \max f(x)$, $x \in [a, b]$, B is a maximum and (B, x) is a minima point.

(7) Determining the tree height. For the convex interval where x (x is the height of the tree) is largest, if there is only one inflection point above the point of maximal value, the x of that maximal point is the tree height(Fig. 5b, d); if there are more than one inflection point above the point of maximal value, there is a concave interval above it, and the x of the point of minimal value of the concave interval is the tree height.

Using the coordinates of point o and point A (Fig. 4), we could calculate the length of the leaning tree. Nevertheless, to ensure consistency with ground-based measurements, the tree heights documented in this study were exclusively calculated as vertical heights, discounting any extra length resulting from the trees' natural inclination.

2.3.4 Approach evaluation

Utilizing point clouds with a height of 1–5 m, we were able to precisely identify the tree trunks of 413 reference trees and their respective center positions individually in the study site through visual interpretation within the TerraSolid and ArcGIS Desktop environments, ultimately achieving the reference dataset. Taking into account the noise level present in the point clouds, the manually pinpointed trunk locations were anticipated to be accurate to 3–5 cm, serving as the ground truth for further analysis. If the distance between the center of a detected tree A and a reference tree B was found to be less than 0.5 m, A and B were considered to be a match. In cases where tree B had two or more potential matches, the tree with the shortest distance was considered the valid match. Three key statistical parameters were utilized to assess the performance of individual tree detection algorithms, namely, "recall" (Re), representing the detection rate of trees; "precision" (Pr), indicating the detection accuracy of identified trees; and "*F*-score," reflecting the overall accuracy, encompassing both omissions and commissions. These three measures were calculated as follows:

$$\mathrm{Re} = TP \big/ (TP + FN) \tag{6}$$

$$\mathrm{Pr} = TP \big/ (TP + FP) \tag{7}$$

$$F - score = 2 \times \frac{Pr \times Re}{Pr + Re} \tag{8}$$

where *TP* represents the matched trees, *FN* is the number of trees are not detected (omission error), *FP* is the number of trees wrongly detected (commission error). Furthermore, we calculated the plane differences between the identified trunk locations and their corresponding ground truth data. Subsequently, we reported the root-mean-square error (RMSE) and the mean distance to measure the detection accuracy quantitatively.

The extraction performance of DBH, tree height (H), and stem volume (VOL) was thoroughly evaluated by comparing UAV measurements or estimations with field measurements, using mean error (bias) and RMSE as metrics. Both absolute error (in cm/m/m^3) and relative error (%) were computed for bias and RMSE to facilitate comparisons of detection performance with other studies. These four statistics were defined as follows:

$$bias = \frac{1}{n}\sum_{i=1}^{n}(y_i - \hat{y}_i) \tag{9}$$

$$RMSE = \sqrt{\frac{1}{n}\sum_{i=1}^{n}(y_i - \hat{y}_i)^2} \tag{10}$$

$$bias(\%) = \frac{bias}{\bar{y}} \times 100 \tag{11}$$

$$RMSE(\%) = \frac{RMSE}{\bar{y}} \times 100 \tag{12}$$

where $\hat{y}_i$ is the UAV-derived attribute, y_i is the field-measure reference attribute, $\bar{y}$ is the mean of y_i, and n is the number of trees.

3 Results

3.1 Accuracy of individual tree truck detection

There were 413 reference trees in the study area, and the algorithm detected 417 tree trunks across the entire region. Specifically, of these 417 detected trees, 380 were accurately identified. At the same time, 33 were overlooked (resulting in omission), and 37 were incorrectly labeled (resulting in commission) (Fig. 6). The algorithm achieved a recall rate of 92.0% for detecting individual trees and a precision of 91.1%, leading to an overall *F*-score of 0.916.

By meticulously and carefully analyzing the missed and wrongly detected trees using TerraSolid and ArcGIS software, we found that several factors contributed to these errors. These included (1) clusters of understory crowns encircling the stems, understory canopies situated at varying height intervals, climbing vines, proximity to two budding trees, and significantly leaning trunks.

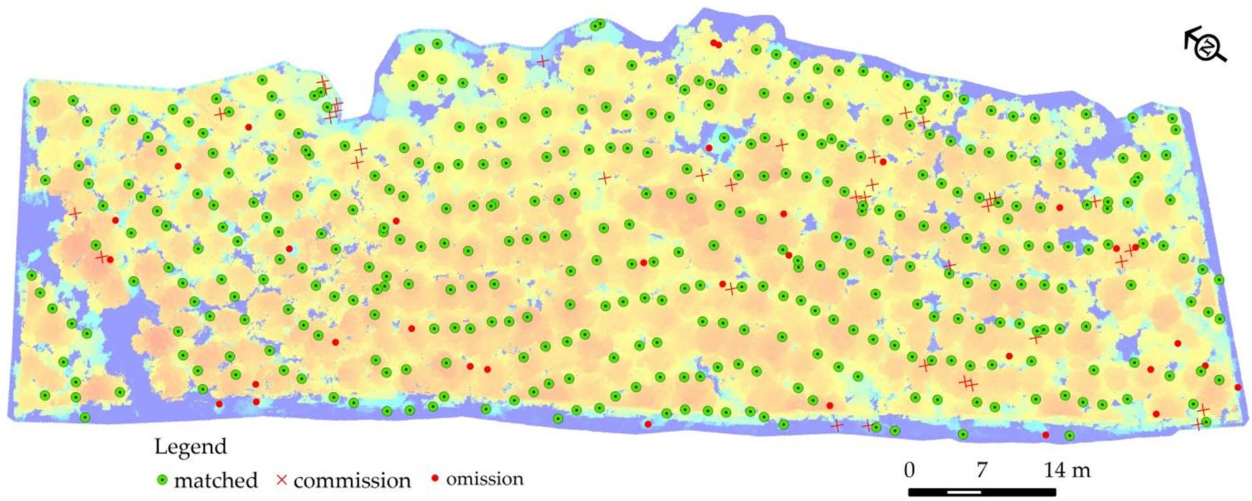

Fig. 6 Comparison of the trunk detection and reference dataset derived by the visual interpretation using 3D point clouds

Collectively, these factors interfered with the point cloud clustering process, leading to variations in the number of clusters at different heights and the geometric positioning of their centers. Consequently, this interference affected the diameter extracted from the point clouds, which were misclassified as non-tree elements and identified as the primary cause of missed detections; (2) the main reason for the incorrect detection of stems was the misidentification of understories or large branches as trees.

Among the 33 field-measured reference trees, the variations in the differences between the x and y coordinates of the detected and field-measured centers spanned from − 22.6 to 8.0 cm and − 16.1 to 10.5 cm, respectively. The average differences were − 0.140 cm for the x-coordinate and − 0.052 cm for the y-coordinate. Furthermore, the RMSE was 15.3 cm for the x-coordinate and 7.9 cm for the y-coordinate. The distance between the detected and measured centers of the trees ranged from 10.0 to 24.4 cm, with an average of 16.9 ± 3.2 cm. It is crucial to note that the measured center of the field-measured reference tree was not precisely at the actual center but on the outer bark and not measured at a similar location. After subtracting the individual trees' radii from the above distances,

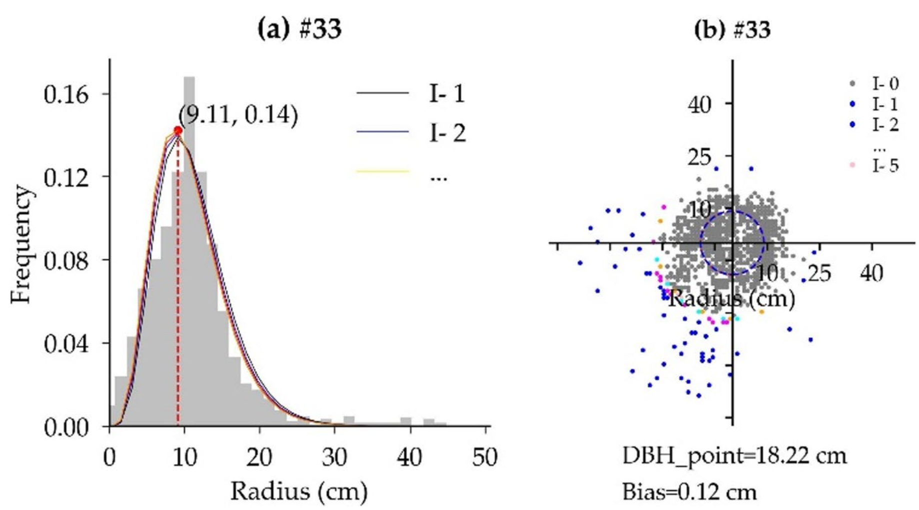

Fig. 7 Process of measuring trunk diameters directly from point clouds via the χ^2-filtering method. (**a**) Changes in the PDF curve of the ^{2}-distribution during the iteration process. Specifically, the red point marks the location of the maximum probability density on this curve. The corresponding x-coordinate (9.11) signifies the radius of the tree trunk. (**b**) Distribution of rejected and retained point clouds on the trunk's cross-section during iterations. The notation I- 1–1–5 refers to the point clouds rejected during iterations 1 through 5, while I- 0 represents the retained point clouds. Additionally, the red circle depicts the circle drawn using the radius of the trunk, and the blue one is the circle drawn using the field-measured diameter

the mean distance between the trees detected and field measurement centers was 9.2 ± 3.4 cm.

3.2 Accuracy of stem diameter measurement

The distance-frequency of point clouds in the trunk's cross-section typically exhibits a χ^2-distribution, characterized by 9 to 12 degrees of freedom. The fitting of the PDF for the χ^2-distribution and the subsequent removing anomalous data was generally accomplished within 2 to 5 iterations (Fig. 7), with a maximum iteration of 29. During the direct measurement of DBH for 33 field-measured reference trees, 30 trees were successfully measured at the standard height of 1.3 m, one at 1.8 m, another at 2.3 m, and one tree could not be directly measured within the height range of 0.8 m to 2.3 m. As a result, its DBH was substituted using the mean value derived from the direct measurements of the remaining 32 trees.

Across all 33 field-measured reference trees, the mean error (bias) of UAV-LiDAR DBH measurements was 2.04% (0.26 cm), and the RMSE was 14.60% (2.18 cm). Notably, the accuracies of UAV-LiDAR diameters measured at 2, 4, and 6 m of the trunk were significantly lower than those of the UAV-LiDAR DBH, evident from the substantially larger bias and RMSE compared to the latter (Table 1).

Scatter plots were computed for cross-validation purposes, contrasting the tree diameters obtained through field measurement with those measured by UAV (Fig. 8). While the UAV-LiDAR-derived DBHs were distributed on both sides of the 1:1 line with residuals showing random dispersion, the deviations from this line were substantial, indicating a less-than-satisfactory agreement between UAV-LiDAR-derived DBH and field-measured DBH (R^2 = 0.37) (Fig. 8a). Furthermore, the UAV-LiDAR-derived diameters at heights of 2.0 m, 4.0 m, and 6.0 m exhibited even more significant deviations from the 1:1 line, with an even poorer correlation between UAV-LiDAR-derived diameters and field-measured diameters (R^2 ranging from 0.17 to 0.26). Notably, most of these points were positioned to the right of the 1:1 line, suggesting overestimation by the UAV-LiDAR measurements (Fig. 8b, c, and d).

When measuring tree diameters using the circle-fitting method, 28 of the 33 field-measured reference trees had diameters greater than 20 cm, resulting in a significant bias (Table 1 and Fig. 9).

The bias and RMSE observed in the DBH measurements obtained using the circle-fitting method were much larger than those extracted using the χ^2-filtering method, which were −50.30% (− 7.64 cm) and 53.92% (8.19 cm), respectively (Table 1). Such a large error is unacceptable in practical application.

After clipping the trunk point clouds with a cylinder having a radius of 0.5 m and a height of 0.5 m, the number of point clouds observed at various heights along the tree stem exhibited minimal variation. Among the 33 field-measured reference trees, the coefficients of variation for the point clouds counts at heights of 1.3, 2.0, 4.0,

Table 1 Bias and root-mean-square error (RMSE) are associated with UAV-diameter measurements at various tree heights, specifically at 1.3 m (DBH), 2 m (D2 m), 4 m (D4 m), and 6 m (D6 m)

Statistics	DBH (circle fitting)	DBH	D2 m	D4 m	D6 m
Bias (%/cm)	− 50.30/− 7.64	− 1.70/− 0.26	− 15.67/− 2.21	− 16.058/− 2.05	6.30/− 0.73
RMSE (%/cm)	53.92/8.19	14.37/2.18	23.16/3.27	24.14/3.08	26.99/3.12

Note: DBH (circle fitting) is the DBH measured with the circle fitting method; DBH, D2 m, D4 m, and D6 m are measured by χ^2-filtering

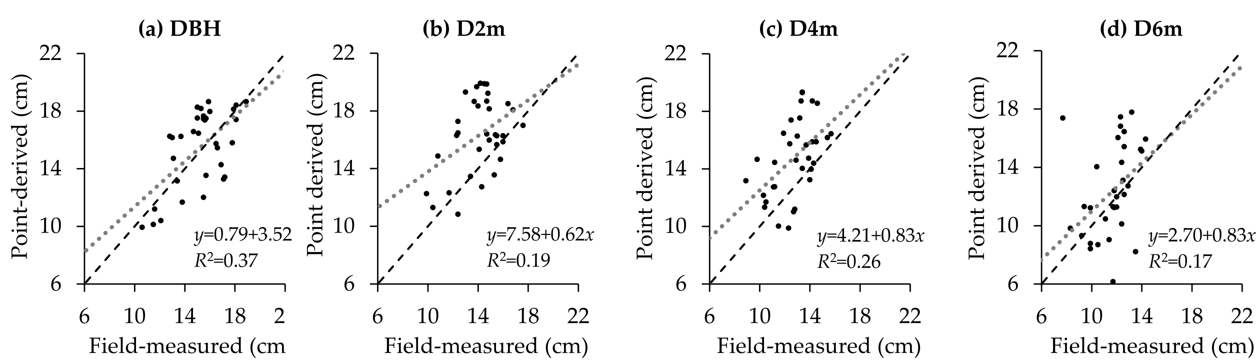

Fig. 8 UAV-LiDAR-derived diameters versus field-measured diameters at heights of 1.3 m (DBH), 2.0 m (D2 m), 4.0 m (D4 m), and 6.0 m (D6 m) of all 33 field-measured reference trees. The black dashed line indicates the 1:1 reference line

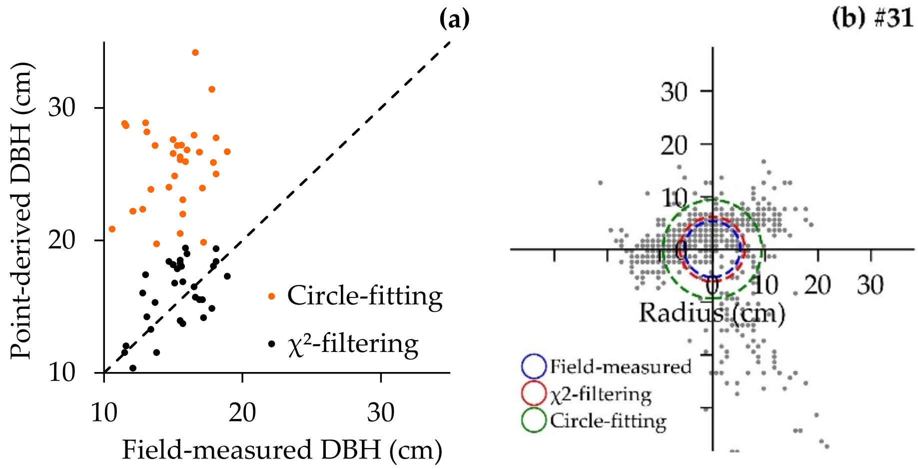

Fig. 9 Comparison of the circle-fitting and χ^2-filtering methods for direct DBH measurement using point clouds. (**a**) Field-measured DBHs versus UAV-LiDAR-derived DBHs using two methods of all field-measured reference trees; (**b**) DBHs obtained by two methods on a trunk's cross-section

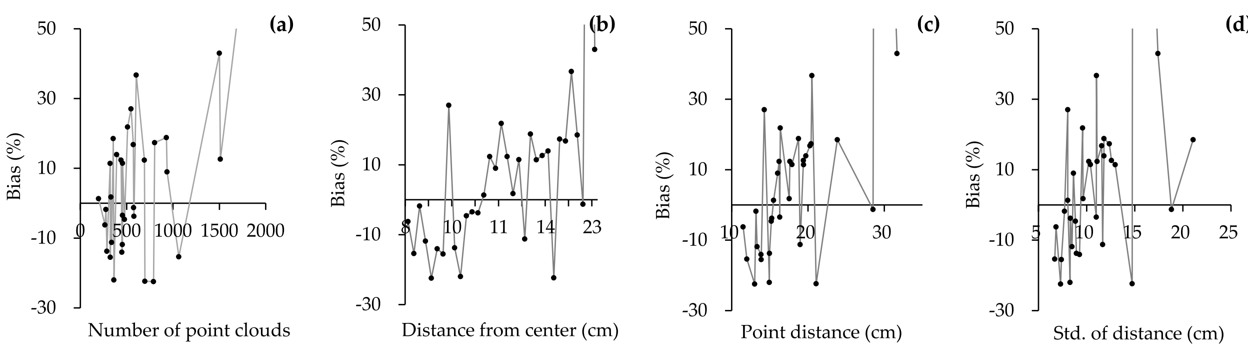

Fig. 10 Relationship between measurement errors of the DBH and the following point cloud statistics: (**a**) the number of point clouds in the trunk cylinders; (**b**) the mean distances between the point clouds and the center of the trunk; (**c**) the mean distances among the point clouds; and (**d**) the standard deviations of the mean distances

and 6.0 m ranged from 0.09 to 0.75. Notably, the coefficients of variation for approximately 70% of the trees fell below 0.5. However, there was a considerable variation in the number of point clouds among the different reference trees. Specifically, at a height of 1.3 m, the point cloud counts ranged from 197 to 2484 points, resulting in a maximum difference of 13 times. Similarly, the maximum difference at a height of 4.0 m also reached eight times.

However, when limiting diameter measurements to a trunk height of 1.3 ± 0.25 m, we found that the accuracy of direct DBH measurements did not exhibit strong correlation with either the number of point clouds in the trunk (Fig. 10a) or the average distance between these point clouds and the trunk's center (Fig. 10b). Furthermore, we also observed no strong correlation between the accuracy of tree DBH measurement and the mean distances among point clouds (Fig. 10c) or the standard deviation of these distances (Fig. 10d). These suggested that the accuracy of the diameter measurement was independent of the dispersion pattern of the laser point clouds.

Upon analyzing the distribution of point clouds within the trunk's cross-section, we observed that:

When the point clouds were concentrated in a circular pattern centered around the trunk's center, the direct DBH measurement was highly accurate (Fig. 11a).

Conversely, if the point cloud distribution was diffuse, the accuracy of the DBH measurement declined (Fig. 11b).

In extreme cases where the point clouds exhibited a highly dispersed and multicentric distribution, the accuracy of the DBH measurement was significantly low (Fig. 11c).

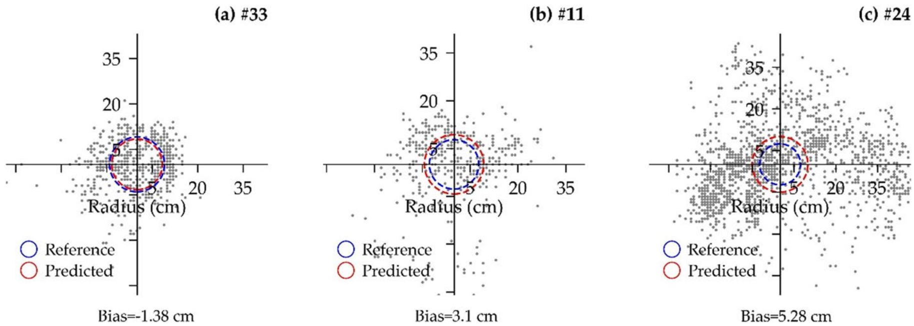

Fig. 11 Distribution pattern of point clouds and bias in direct DBH measurements

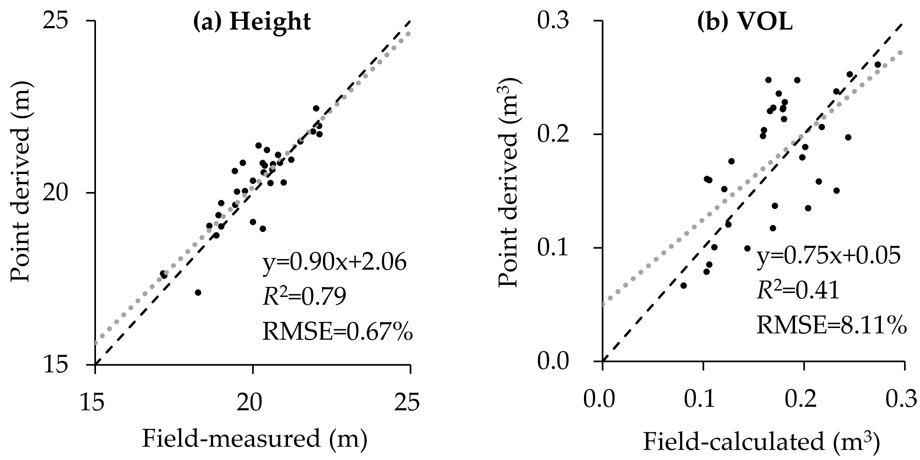

Fig. 12 Scatter plots between the field measurement and UAV-derived individual tree height (**a**) and stem volume (**b**)

3.3 Accuracy of tree height estimations

Out of the 33 field-measured reference trees, the biases for tree height measurements using 3D point clouds ranged from −7.53 to 6.94%, equivalent to −1.43 to 1.18 m, with a mean bias of −0.01% (− 0.01 m) and an RMSE of 2.69% (0.31 m). There were good agreements between UAV-LiDAR-derived tree heights and field-measured tree heights (R^2 = 0.79), and their relationships were close to the 1:1 line (Fig. 12a).

Stem volume is often one of the critical outputs of forest inventory. Utilizing the direct DBH and tree height measurements, stem volumes (VOL) were calculated using Eq. (1). The estimation biases for UAV-derived VOL varied from −35.8% to 55.3%, with a mean bias of 5.00% and an RMSE of 25.09%. The UAV-LiDAR-derived VOL relationships deviated slightly from the 1:1 line. However, the agreement between the UAV-LiDAR-derived VOL and field-calculated VOL was still better than that of the UAV-LiDAR-derived DBH and field-measured DBH (Figs. 12b and 8a). The UAV-LiDAR-derived measurement error for tree height was notably smaller than that of DBH. Applying the principle of error propagation, we hypothesized that the leading cause of estimation inaccuracies in stem volume originated from errors in DBH measurements.

4 Discussion

In this study, we introduced an innovative framework for the automatic and direct extraction of individual tree attributes, including tree number and location, diameter, and height, utilizing low-cost UAV-LiDAR point clouds. This framework employed HDBSCAN algorithms to detect tree trunks and ascertain the number of trees. Additionally, it utilized the probability density function of ^{2}-distribution for filtering point clouds to measure tree diameters and pinpoint tree locations. Furthermore, the framework extracted tree heights through pseudo-waveforms. Our results demonstrated that this framework offered an efficient solution for automated plantation forest inventory. Notably, to our best knowledge, this marked a pioneering effort where individual tree diameters were directly measured using a ^{2}-filtering method, and tree heights were determined through pseudo-waveforms. This study also demonstrated for the first time that the classical circle-fitting method was unsuitable for tree diameter measurement using low-cost UAV-LiDAR data.

4.1 Crown detection versus tree trunk detection

The accuracy of individual tree detection through top-down canopy segmentation was found to be limited, primarily due to the significant overlap and complex interlacing of the canopy (Yu et al. 2024; Yan et al. 2024; Zhang et al. 2022a; Liu et al. 2023; Xiang et al. 2024). Given that tree trunks are distinctly separated, bottom-up trunk detection and segmentation techniques emerge as a feasible approach to overcome the difficulties associated with canopy segmentation. The stem or trunk detection approach significantly enhances detection accuracy in scenarios where point cloud density is substantial. For instance, Neuville et al. (2021) employed the HDBSCAN algorithm to detect tree trunks, achieving an *F*-score of 0.89 under leaf-off conditions. Similarly, Lin et al. (2021) introduced a bottom-up approach for individual tree localization and segmentation, leveraging 2D peak detection and Voronoi diagrams. This method proved effective under deciduous and partially deciduous cover, achieving overall single tree detection accuracies of 0.98 and 0.88, respectively, with point densities of 5500 and 4500 pts·m^{-2} (at the 75 th percentile) in broad-leaved forests with a tree density of 5× 2.5 m. Remarkably, even with moderate point cloud densities ranging from 400 to 1264 pts·m^{-2}, Deng et al. (2024) achieved excellent segmentation results (*F*-score of 0.92 to 1.00) for detecting Eucalyptus young forests of 1, 2, and 4 years old. In recent years, deep learning algorithms such as PointNet, CNN, YOLO, and ForAINet have emerged as focal points for LiDAR-based individual tree segmentation (Kim et al. 2023; Sun et al. 2023; Xiang et al. 2024; Straker et al. 2023). Hence, there is an urgent requirement for future research to confirm the effectiveness of these algorithms in detecting trunks within Eucalyptus plantations.

One of the most significant challenges in trunk detection is minimizing the interference caused by foliage and understory vegetation. Considering the biological traits of tree species and the forest structure, rationally determining the height interval of point cloud segmenting in the trunk layer is an important measure to mitigate the above impacts. Thanks to the algorithm we developed, we could quickly perform trunk segmentation experiments with various height slices in this study. Ultimately, our finding revealed that point clouds with a height interval of 2–4 m were optimal for trunk detection. The results indicated that the height interval for trunk layer segmentation was not fixed and must be determined based on the specific forest structural contexts.

The diameter of the understory vegetation canopy is usually more significant than the diameter of the forest trees. Therefore, to minimize these effects, we employed a technique involving the extraction of trunk diameters from trunk slices, followed by determining the stem based on these measurements. By leveraging the HDBSCAN algorithm for point cloud clustering at the trunk level, our study successfully achieved accurate individual tree detection through this methodology. The detection precision reached 91.1%, with an accompanying *F*-score of 0.916. Taking into account the density of forest trees and the structural features of the understory vegetation within the study area, we deem this level of accuracy as satisfactory and sufficient to meet the demands of precise forestry management. Furthermore, Kukkonen et al. (2022) further assert that integrating segmented tree trunks and crowns enhances individual tree detection's precision and guides future research in a promising direction.

4.2 Statistical distribution of point clouds and direct tree diameter measurement

For survey-grade laser scanners encompassing terrestrial, mobile, and UAV-based systems, the laser point clouds that reflects from a tree trunk exhibits a hollow circle or circular arc when projected onto the (x, y) plane, as noted by Čerňava et al. (2019). Consequently, the current practice of directly measuring tree diameters with LiDAR data often involves utilizing a sample circle-fitting method and its evolutionary approach (Xiang et al. 2024; Brede et al. 2017). Despite the advancements in UAV-LiDAR technology, the direct measurement of individual tree diameters using this data still needs the desired level of accuracy, regardless of whether it involves survey-grade or low-cost scanners. In their respective studies, Brede et al. (2017) and Xiang et al. (2024) employed survey-grade scanners to measure tree DBH directly, achieving RMSEs of 4.24 cm (at a point cloud density of 140 pts·m^{-2}) and 5–10 cm (at 9529 pts·m^{-2}), respectively. Regarding low-cost UAV-LiDAR, Kuželka et al. (2020) yielded an RMSE range of 17–20%. Krůček et al. (2020) reported a residual standard error (RSE) of 8.91 cm with a point cloud density of 4387 pts·m^{-2}. Neuville et al. (2021) employed principal component analysis to estimate DBH, achieving RMSEs of 15 cm and 19 cm for leaf-on and leaf-off conditions, respectively. Jaakkola et al. (2017) achieved RMSEs of 5.5 cm (22.12%) and 6.8 cm (27.46%) at a point cloud density of 800 pts·m^{-2}, employing principal component analysis (PCA) and circle fitting methods, respectively. Various factors hamper the accuracy of UAV-LiDAR tree diameter measurements. These factors encompass the sparsity and noise present in the point clouds surrounding tree trunks (Xiang et al. 2024), ranging and orientation errors, the significant divergence of the laser beam, and the specific processing algorithm utilized (Jaakkola et al. 2017). We proposed that the primary cause of the reduced accuracy in direct tree diameter measurements obtained by low-cost UAV-LiDAR (Table 1 and Fig. 9) stemmed from the fact that the point clouds generated by such systems exhibited a solid-circle distribution in the trunk cross-section rather than a hollow circle or arcs (Figs. 3b, 7b, 9b, and 11). This deviation led to an absence of a mathematical foundation for employing the circle-fitting method to measure tree diameters.

The Matrice 300 RTK UAS system employed in this study boasts a manufacturer-stated accuracy of 0.1 m per 50 m horizontally and 0.05 m vertically (standard deviation) for the DJI Zenmuse L1 scanning system. Specifically, the laser scanner's distance measurement precision (RMS 1σ) is 3 cm at a 100 m distance (DJI 2024). A recent test revealed that, at a height of 10 m, the estimated x and y differences using the UAV's attitude were 0.13 m and 0.04 m, respectively, with standard deviations of 0.05 m and 0.02 m. The horizontal discrepancy intensifies as altitude increases (Czyża et al. 2023). In forest environments, the Zenmuse L1 system achieves an elevation accuracy (RMSE) of 0.044–0.065 m when flying at 100 m (Stroner et al. 2023).

When projecting the point clouds within the trunk cylinder onto the (x, y) plane, it assumed a near-solid circular shape (Figs. 3b, 7b, 9b, and 11), as a result, the accuracy of diameter measurement using the circle fitting method was very low (Table 1). To analyze these point clouds, we employed the following techniques:

(1) A thin cube (sheet) with a length width height equal to 50 cm 5 cm 50 cm was used to crop the point clouds on the trunk, centered on the center of the trunk cross-section at the height of 1.3 m of the tree (Fig. 13a), and calculating the mean x-coordinate ($x_0 = \frac{1}{n}\sum_{i=1}^{n} x_i$), where n represents the number of point clouds and x_0 marks the trunk's central x-coordinates.
(2) Computing the one-dimensional horizontal-plane distances ($d(i)$) between point clouds and the trunk center, $d(i) = x_i - x_0$, along with the maximum distance ($d_{\max}$).
(3) Dividing the distance interval $[0, d_{\max}]$ into 30 equal segments and tallying the point cloud frequencies in each segment to generate a distance-frequency histogram (bilateral).

The results indicated that although the number of point clouds was small, with a mean (standard deviation) of 635.5 ±459.4 pts·m^{-2}, most reference trees exhibited bimodal histograms, with the dividing line close to the trunk's center and the two peaks positioned near the bark (Fig. 13b).

For laser scanners with notable errors in point cloud positioning, similar to the one utilized in this study, if the point cloud density is high and the trunk diameter exceeds the error margin, we posit that when projecting the trunk's point clouds onto the (x, y) plane in a particular direction, the point clouds exhibit a normal distribution centered on the bark. Specifically, the frequency (density) of points is highest at the bark and gradually tapers off to zero on both sides. We computed the two-dimensional planar distances from all these points to the trunk's center, segmented the maximum distance into 50 equal intervals, and tallied the frequencies within each interval to generate a two-dimensional distance-frequency histogram (Fig. 13c).

Based on the observations above, we postulate that if the positional error of the point cloud is less than the tree trunk's radius, the trunk's point cloud histograms are

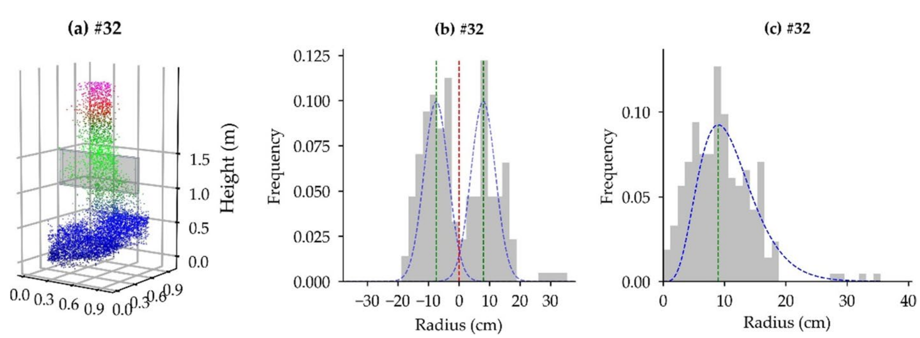

Fig. 13 Cubic clipping and histogram analysis of point clouds on a tree trunk. (**a**) Clipping point clouds with a thin cube. One- and two-dimensional distance-frequency histograms (**b** and **c**) of the point clouds. The red and green dashed vertical lines in (**b**) and (**c**) indicate the locations of the trunk center and bark, respectively, as simulated from field-measure DBH. The blue dashed curves in (**b**) and (**c**) are the simulated curves of normal and χ^2-distribution, respectively

distinct, meaning that the one-dimensional distance-frequency histogram follows two separate normal distributions. Similarly, the two-dimensional distance-frequency histogram also adheres to a normal distribution. Conversely, suppose the positional error of the point cloud is smaller than the tree's diameter but more significant than its radius; the one-dimensional distance-frequency histogram conforms to two normal distributions that intersect (Fig. 13b). The two-dimensional distance-frequency histogram conforms to the ^{2}-distribution (Fig. 13c). Based on this assumption, we fitted the histograms using the corresponding PDF and refined our trunk diameter measurements by eliminating anomalous point clouds (Fig. 7). Although we recognize that our diameter measurements, with a RMSE of 14.6% (2.18 cm) (Table 1), still have room for improvement, they nonetheless surpass the results obtained in most previous studies, e.g., Jaakkola et al. (2017), Kukkonen et al. (2017), Kuželka et al. (2020), Neuville et al. (2021), and Xiang et al. (2024). Therefore, the approach proposed in this paper for direct measurement of tree diameters using 3D point clouds is reliable and has a solid mathematical foundation. Our future efforts will verify the above hypothesis, unravel the factors contributing to measurement inaccuracies and refine our algorithm to achieve greater precision. Furthermore, given the increased inefficiencies and expenses associated with high-density point clouds in UAV-LiDAR data collection and preprocessing, we also intend to explore how point cloud density impacts diameter measurement accuracy, aiming to optimize density to reduce data acquisition costs.

Specific experimental outcomes revealed that when utilizing the under-canopy UAV-LiDAR, the RMSE for direct DBH extraction in sparse and obstructed plots stood at 0.60 cm (2.2%) and 0.92 cm (3.1%), respectively. Moreover, the integration of under- and above-canopy UAVs led to an RMSE of 10.1% for stem volume estimation, as reported by Hyyppä et al. (2020a). This figure is considerably higher than when only the above-canopy UAV is employed. Therefore, this approach merits further exploration in subsequent research endeavors.

4.3 Tree height estimation consistent with field measurement

The height of a tree is defined as the vertical distance between its tallest point and the base where it meets the ground. In UAV-LiDAR tree height measurements, both CHM-based tree height determinations (e.g., Liao et al. 2022; Ganz et al. 2019; Hyyppä et al. 2020a) and 3D point cloud-derived measurements (e.g., Krůček et al. 2020; Hyyppä et al. 2020b) exhibited excellent accuracy, typically yielding an RMSE of less than 5%. However, the measurement method for the reference tree's height significantly influenced the accuracy evaluation. Liao et al. (2022) found that altimeter (telescopic pole) measurements exhibited a bias ranging from −4.8 to −6.7% and an RMSE of 9.0% to 9.9%, significantly underperforming compared to UAV-CHM measurements and post-felling measurements. Similarly, Ganz et al. (2019) concluded that altimeter (Vertex IV hypsometer) measurements were less accurate than UAV-CHM extractions. Krause et al. (2019) observed that altimeter (hypsometer) measurements overestimated tree height with a bias of 0.86% and an RMSE of 1.82%, while photogrammetric CHM measurements underestimated it with a bias of −0.81% and an RMSE of 2.07%. Therefore, when validating the accuracy of UAV-LiDAR tree height measurements, it is advisable to fall the trees for reference tree height measurements, if conditions permit, to ensure the highest level of accuracy.

A critical issue to consider for tree height measurements is the determination of the top center of the crown. The trees were not uniformly perpendicular to the ground; most were tilted at various angles. In our study, the Eucalyptus forests featured tall, slender trunks leaning at significant angles, particularly those positioned at the edges of the stands. These trees displayed a pronounced offset, where the canopy's top center deviated from the trunk base's center by over 1 m. Consequently, for precise individual tree segmentation relying on trunk detection, pinpointing the exact location of the crown's top center becomes paramount for accurate tree height measurements. We used the center coordinates at 1.3 m and 7.0 m of the trunk and CHM to calculate the centers' positions at the top of the canopy (Fig. 4). Following this, we extracted the tree height by segmenting individual trees using a cylindrical clipping of the point clouds with a 0.75 m radius. This methodology allowed us to gauge the accuracy of our tree height measurements efficiently.

Another essential issue to consider when measuring tree height is its application scenario. One of the crucial applications of tree height measurements lies in estimating stem volume and biomass. Traditionally, when collecting data for modeling these parameters, tree height is measured after falling using a tape on the trunk in China. However, accurately determining the topmost point of a tree, whether by using an altimeter for standing trees or a tape measure for felled ones, is challenging. The actual measured height often falls short of the tree's accurate height. To ensure precision in estimating standing tree volume and biomass, UAV-LiDAR measurements of individual tree heights must align as closely as possible with actual field measurements. In our study, we identified the extreme value of the highest convex interval in the height-frequency pseudo-waveforms of the point clouds rather than just the highest *z*-value as the tree height. This extreme point signifies the position with the densest foliage distribution in the topmost layer of the tree or the interface between the second-to-top and topmost layers, and it is identified as the highest point of the tree by the surveyor. This approach ensures that the start of the UAV-LiDAR measurements is consistent with field measurements. The results showed a minimal bias of − 0.01% (− 0.01 m) in our tree height measurements and an RMSE of 2.69% (0.31 m), indicating that we have successfully achieved our objectives. It is worth noting that while we can directly measure the actual length of leaning trees based on their growth direction (Fig. 4), we still used the vertical height in this study to maintain consistency with field measurements.

4.4 Application of the proposed framework

This study was conducted in a relatively simplistic structure of Eucalyptus plantation forests. The subject was a single-story forest with a canopy characterized by a relatively spare distribution of twigs and leaves. Based on our extensive UAV-LiDAR dataset covering 4700 ha with a density of 350 pts m^{-2} in the same region, the average canopy cover of the Eucalyptus plantations was 0.80, which was notably lower compared to the canopy cover of the planted Chinese fir forests (0.96), Masson pine forests (0.94), and broad-leaved forests (0.95). Given that LiDAR point clouds are unable to penetrate canopy material, we believe that the individual-tree segmentation framework proposed in this paper is likely only applicable to Eucalyptus plantation forests and planted forests with simpler and sparser structures and not to natural forests. Further experimentation is necessary to assess the adaptability of this framework.

A key factor contributing to the success of this study is the ultra-high density of the point clouds. Regrettably, we were unable to ascertain the minimum point cloud density required. Nevertheless, we hypothesize that a density of at least approximately 20,000 pts m^{-2} or even higher is necessary to ensure adequate reflection of point clouds from the tree trunk for segmentation. Furthermore, factors such as flight altitude, scanning angle, and route planning also significantly impact the quality of the point cloud, and these aspects require further investigation in future studies.

The fundamental premise of the diameter measurement method introduced in this paper is that the cross-section of the trunk is circular. Nevertheless, as Wang et al. (2017) pointed out, the trunk cross-section is never perfectly circular. When the shape of the trunk cross-section deviates significantly from a circle, it is inadvisable to apply the method proposed herein. Instead, alternative methods such as iterative Fourier series approximation (Wang et al. 2017) or the convex hull algorithm (You et al. 2016) should be employed.

5 Conclusion

This paper introduced a novel framework for automatically and directly measuring individual tree attributes, leveraging ultra-high-density point clouds collected by low-cost UAV-LiDAR. The framework exhibited outstanding performance in Eucalyptus plantations, the largest planted broad-leaved forests globally. Furthermore, our study indicated that the classical circle-fitting method might not be adequate for directly measuring tree diameter using low-cost UAV-LiDAR data.

The HDBSCAN algorithm efficiently clusters point clouds in the trunk layer. By clipping the trunk layer point clouds at an appropriate height interval from the normalized version, we effectively minimized the impact of foliage and understory vegetation on tree trunk detection. Using a probability density function of ^{2}-distribution to filter the noise point clouds, we accurately determined the diameters at various height slices along the trunks. These diameters facilitated precise identification of the number of tree stems and calculation of their approximate locations. The point clouds centered around the trunk exhibited a normal distribution, with the bark as its focal point. Upon calculating the distances from the point clouds to the trunk center and generating a distance-relative frequency histogram, it became evident that the point clouds follow a χ^2-distribution. Therefore, by segmenting the trunk's point clouds using a cylinder, we could directly extract the diameters of the tree stems at different heights and their accurate position after filtering the point clouds. The coordinates of the crown's topmost center could be precisely calculated using the coordinates of the trunk centers at 1.3 m and 7.0 m, along with CHM. By cylindrical segmenting the point clouds of the tree crown, we could extract the tree height using pseudo-waveforms, ensuring consistency between the extracted results and field measurements.

The relevant algorithms presented in this paper require further optimization, and additional experiments in various forest contexts are necessary to verify the adaptability of the framework proposed in this paper.

Acknowledgements
The authors sincerely express their gratitude to Chengling Yang, Jinfeng Jiang, Zhihao Long, Xin Lin, Yao Liang, and Zhengfeng Liu from the Guangxi Forest Inventory and Planning Institute (FIPI-GX), as well as Dr. Kai Su and Xiangbei Zhou from the Forest College of Guangxi University, for their valuable contributions in UAV-LiDAR data collection and fieldwork. Additionally, we extend our appreciation to the anonymous reviewers and the editors for their thoughtful recommendations.

Code availability
The codes developed for the current study are available from the corresponding author on reasonable request.

Authors' contributions
MZ: methodology, formal analysis, investigation, data curation, writing—original draft. CL: conceptualization, methodology, formal analysis, writing—original draft and—review and editing, project administration, funding acquisition. ZL: investigation, data curation, funding acquisition. The authors read and approved the final manuscript.

Funding
This work received financial support from the Forestry Department of Guangxi Zhuang Autonomous Region, China (GXLY2020 KT02), and the Guangxi Forest Inventory and Planning Institute (GXFIPI-KY202401).

Data availability
The data that support the findings of this study are available at https://doi.org/10.57760/sciencedb.14659.

Ethics approval consent to participate
Not applicable.

Consent for publication
All authors gave their informed consent to this publication and its content.

Competing interests
The authors declare that they have no competing interests.

Author details
[1]School of Computer, Electronic and Information, Guangxi University, 100 East Daxue Rd., Nanning 530004, China. [2]Forestry College, Guangxi University, 100 East Daxue Rd., Nanning 530004, China. [3]Guangxi Forest Inventory & Planning Institute, 14 Zhonghua Rd., Nanning 530011, China.

Received: 23 October 2024 Accepted: 4 April 2025
Published online: 12 May 2025

References

Ayrey E, Fraver S, Kershaw JA, Kenefic LS, Hayes D, Weiskittel AR, Roth BE (2017) Layer stacking: A novel algorithm for individual forest tree segmentation from LiDAR point clouds. Can J Remote Sens 43:16–27. https://doi.org/10.1080/07038992.2017.1252907
Brede B, Lau A, Bartholomeus HM, Kooistra L (2017) Comparing RIEGL RiCOPTER UAV LiDAR derived canopy height and DBH with terrestrial LiDAR. Sensors 17:2371. https://doi.org/10.3390/s17102371
Cárdenas JL, López A, Ogayar CJ, Feito FR, Juan M, Jurado JM (2022) Reconstruction of tree branching structures from UAV-LiDAR data. Front Environ Sci 10:960083. https://doi.org/10.3389/fenvs.2022.960083
Čerňava J, Mokroš M, Tucček J, Antal M, Slatkovská Z (2019) Processing chain for estimation of tree diameter from GNSS-IMU-based mobile laser scanning data. Remote Sens 11:615. https://doi.org/10.3390/rs11060615
Czyża S, Szuniewicz K, Kowalczyk K, Dumalski A, Ogrodniczak M, Zieleniewicz L (2023) Assessment of accuracy in unmanned aerial vehicle (UAV) pose estimation with the real-time kinematic (RTK) method on the example of DJI Matrice 300 RTK. Sensors 23:2092. https://doi.org/10.3390/s23042092
d'Oliveira MVN, Broadbent EN, Oliveira LC, Almeida DRA, Papa DA, Ferreira ME, Zambrano AMAA et al (2020) Aboveground biomass estimation in Amazonian tropical forests: a comparison of aircraft- and GatorEye UAV-borne LiDAR data in the Chico Mendes Extractive Reserve in Acre. Brazil Remote Sens 12:1754. https://doi.org/10.3390/rs12111754
Dainelli R, Toscano P, Di Gennaro SF, Matese A (2021) Recent advances in unmanned aerial vehicle forest remote sensing—A systematic review. Forests 12:327. https://doi.org/10.3390/f12030327
Dalla Corte AP, Rex FE, Almeida DRA, de Sanquetta CR, Silva CA, Moura MM et al (2020) Measuring individual tree diameter and height using GatorEye high-density UAV-Lidar in an integrated crop-livestock-forest system. Remote Sens 12(5):863. https://doi.org/10.3390/rs12050863
Deng S, Xu Q, Yue Y, Jing S, Wang Y (2024) Individual tree detection and segmentation from unmanned aerial vehicle-LiDAR data based on a trunk point distribution indicator. Comput Electron Agr 218:108717. https://doi.org/10.1016/j.compag.2024.108717
Dersch S, Heurich M, Krueger N, Krzystek P (2021) Combining graph-cut clustering with object-based stem detection for tree segmentation in highly dense airborne lidar point clouds. ISPRS J Photogrammet Remote Sen 172:207–222. https://doi.org/10.1016/j.isprsjprs.2020.11.016
DJI (2024) M300 RTK User Manual CHS v3.4.pdf.https://dl.djicdn.com/downloads/matrice-300/20230526UM/M300_RTK_User_Manual_CHS_v3.4.pdf. [2024–04–20].
Fu Y, Niu Y, Wang L, Li W (2024) Individual-tree segmentation from UAV–LiDAR data using a region-growing segmentation and supervoxel-weighted fuzzy clustering approach. Remote Sens 16:608. https://doi.org/10.3390/rs16040608
Ganz S, Käber Y, Adler P (2019) Measuring tree height with remote sensing—A comparison of photogrammetric and LiDAR data with different field measurements. Forests 10:694. https://doi.org/10.3390/f10080694
Guo Q, Su Y, Hu T, Guan H, Jin S, Zhang J, Zhao X, Xu K, Wei D, Kelly M, Coops N (2020) Lidar boosts 3D ecological observations and modeling: A review and perspective. IEEE Geosci Rem Sen M 232–257:232. https://doi.org/10.1109/MGRS.2020.3032713
Gupta S, Weinacker H, Koch B (2010) Comparative analysis of clustering-based approaches for 3-D single tree detection using airborne fullwave lidar data. Remote Sens 2:968–989. https://doi.org/10.3390/rs2040968
Hakula A, Ruoppa L, Lehtomäki M, Yu X, Kukko A, Kaartinen H, Taher J et al (2023) Individual tree segmentation and species classification using high-density close-range multispectral laser scanning data. ISPRS Open J Photogramm Remote Sens 9:100039. https://doi.org/10.1016/j.ophoto.2023.100039
Hu T, Sun X, Su Y, Guan H, Sun Q, Kelly M, Guo Q (2021) Development and performance evaluation of a very low-cost UAV-Lidar system for forestry applications. Remote Sens 13:77. https://doi.org/10.3390/rs13010077
Hua LS, Chen L. W, Antov P, Kristak L, Tahir, PM (2022) Engineering Wood Products from Eucalyptus spp. Adv Mater Sci Eng 8000780. https://doi.org/10.1155/2022/8000780
Hyyppä E, Hyyppä J, Hakala T, Kukko A, Wulder MA, White JC, Pyörälä J et al (2020) Under-canopy UAV laser scanning for accurate forest field measurements. ISPRS J Photogramm Remote Sens 164:41–60. https://doi.org/10.1016/j.isprsjprs.2020.03.021
Hyyppä E, Kukko A, Kaijaluoto R, White JC, Wulder MA, Pyörälä J, Liang X et al (2020) Accurate derivation of stem curve and volume using backpack mobile laser scanning. ISPRS J Photogramm Remote Sens 161:246–262. https://doi.org/10.1016/j.isprsjprs.2020.01.018
Jaakkola A, Hyyppä J, Kukko A, Yu X, Kaartinen H, Lehtomäki M, Lin Y (2010) A low-cost multi-sensoral mobile mapping system and its feasibility for tree measurements. ISPRS J Photogramm Remote Sens 65:514–522. https://doi.org/10.1016/j.isprsjprs.2010.08.002
Jaakkola A, Hyyppä J, Yu X, Kukko A, Kaartinen H, Liang X, Hyyppä H, Wang Y (2017) Autonomous collection of forest field reference—The outlook and a first step with UAV laser scanning. Remote Sens 9:785. https://doi.org/10.3390/rs9080785
Jeronimo SMA, Kane VR, Churchill DJ, McGaughey RJ, Franklin JF (2018) Applying LiDAR individual tree detection to management of structurally diverse forest landscapes. J for 116:336–346. https://doi.org/10.1093/jofore/fvy023
Kim D-H, Ko C-U, Kim D-G, Kang J-T, Park J-M, Cho H-J (2023) Automated segmentation of individual tree structures using deep learning over LiDAR point cloud data. Forests 14:1159. https://doi.org/10.3390/f14061159
Krause S, Sanders TGM, Mund J-P, Greve K (2019) UAV-based photogrammetric tree height measurement for intensive forest monitoring. Remote Sens 11:758. https://doi.org/10.3390/rs11070758
Krůček M, Král K, Cushman KC, Missarov A, Kellner JR (2020) Supervised segmentation of ultra-high-density drone lidar for large-area mapping of individual trees. Remote Sens 12:3260. https://doi.org/10.3390/rs12193260
Kukkonen M, Maltamo M, Korhonen L, Packalen P (2022) Evaluation of UAS LiDAR data for tree segmentation and diameter estimation in boreal forests using trunk- and crown-based methods. Can J For Res 52:674–84. https://doi.org/10.1139/cjfr-2021-0217

Kuželka K, Slavík M, Surový P (2020) Very high density point clouds from UAV laser scanning for automatic tree stem detection and direct diameter measurement. Remote Sens 12:1236. https://doi.org/10.3390/rs12081236
Lee Y, Lee J (2024) Evaluation of accuracy in estimating diameter at breast height based on the scanning conditions of terrestrial laser scanning and circular fitting algorithm. Forests 15:313. https://doi.org/10.3390/f15020313
Li W, Guo Q, Jakubowski MK, Kelly M (2012) A new method for segmenting individual trees from the lidar point cloud. Photogramm Eng Remote Sens 78(1):75–84. https://doi.org/10.14358/PERS.78.1.75
Li J, Yang B, Cong Y, Cao L, Fu X, Dong Z (2019) 3D forest mapping using a low-cost UAV laser scanning system: Investigation and comparison. Remote Sens 11:717. https://doi.org/10.3390/rs11060717
Li C, Chen Z, Zhou X, Zhou M, Li Z (2023) Generalized models for subtropical forest inventory attribute estimations using a rule-based exhaustive combination approach with airborne LiDAR-derived metrics. Gisci Remote Sens 60(1):2194601. https://doi.org/10.1080/15481603.2023.2194601
Liang X, Wang Y, Pyrl J, Lehtomki M, Yu X, Kaartinen H, Kukko A. et al. (2019) Forest in situ observations using unmanned aerial vehicle as an alternative of terrestrial measurements. For Ecosyst 6(20). https://doi.org/10.1186/s40663-019-0173-3
Liao K, Li Y, Zou B, Li D, Lu D (2022) Examining the role of UAV Lidar data in improving tree volume calculation accuracy. Remote Sens 14:4410. https://doi.org/10.3390/rs14174410
Lin Y-C, Liu J, Fei S, Habib A (2021) Leaf-off and leaf-on UAV LiDAR surveys for single-tree inventory in forest plantations. Drones 5:115. https://doi.org/10.3390/drones5040115
Lin J, Chen D, Yang S, Liao X (2023) Precise aboveground biomass estimation of plantation forest trees using the novel allometric model and UAV-borne LiDAR. Front for Glob Change 6:1166349. https://doi.org/10.3389/ffgc.2023.1166349
Liu T, Im J, Quackenbush LJ (2015) A novel transferable individual tree crown delineation model based on Fishing Net Dragging and boundary classification. ISPRS J Photogramm Remote Sens 110:2. https://doi.org/10.1016/j.isprsjprs.2015.10.002
Liu C, Xing Y, Duanmu J, Tian X (2018) Evaluating different methods for estimating diameter at breast height from terrestrial laser scanning. Remote Sens 10:513. https://doi.org/10.3390/rs10040513
Liu Y, You H, Tang X, You Q, Huang Y, Chen J (2023) Study on individual tree segmentation of different tree species using different segmentation algorithms based on 3D UAV data. Forests 14:1327. https://doi.org/10.3390/f14071327
López-Amoedo A, Silvosa MR, Lago MB, Lorenzo H, Acuña-Alonso C, Álvarez X (2023) Weight estimation models for commercial *Pinus radiata* wood in small felling stands based on UAV-LiDAR data. Trees, Forests and People 14:100436. https://doi.org/10.1016/j.tfp.2023.100436
Maas H-G, Bienert A, Scheller S, Keane E (2008) Automatic forest inventory parameter determination from terrestrial laser scanner data. Int J Remote Sens 29:1579–93.https://doi.org/10.1080/01431160701736406
Maesano M, Santopuoli G, Moresi FV, Matteucci G, Lasserre B, Mugnozza GS (2022) Above ground biomass estimation from UAV high resolution RGB images and LiDAR data in a pine forest in southern Italy. iForest 15:451–457. https://doi.org/10.3832/ifor3781-015
Maltamo M, Packalen P (2014) Species-specific management inventory in Finland. Chapter 12 in Maltamo M, Naset E, Vauhkonen J (eds) Forestry applications of airborne laser scanning: Concepts and case studies. Springer, Dordrecht. p 464
McGaughey RT, Kruper A, Bobsin CR, Bormann BT (2024) Tree species classification based on upper crown morphology captured by uncrewed aircraft system lidar data. Remote Sens 16:603. https://doi.org/10.3390/rs16040603
Mongus D, Žalik B (2015) An efficient approach to 3D single tree-crown delineation in LiDAR data. ISPRS J Photogramm Remote Sens 108:219–233. https://doi.org/10.1016/j.isprsjprs.2015.08.004
Muss JD, Mladenoff DJ, Philip A, Townsend PA (2011) A pseudo-waveform technique to assess forest structure using discrete lidar data. Remote Sens Environ 115:824–835. https://doi.org/10.1016/j.rse.2010.11.008
Næsset E (2002) Predicting forest stand characteristics with airborne scanning laser using a practical two-stage procedure and field data. Remote Sens Environ 80:88–99. https://doi.org/10.1016/S0034-4257(01)00290-5
Næsset E, Bjerknes K-O (2001) Estimating tree heights and number of stems in young forest stands using airborne laser scanner data. Remote Sens Environ 78:328 /340. https://doi.org/10.1016/S0034-4257(01)00228-0
Næsset E, Gobakken T, Holmgren J, Hyyppä HHJ, Maltamo M, Nilsson M, Olsson H et al (2004) Laser scanning of forest resources: the nordic experience. Scand J for Res 19(6):482–499. https://doi.org/10.1080/02827580410019553
Neuville R, Bates JS, Jonard F (2021) Estimating forest structure from UAV-mounted LiDAR point cloud using machine learning. Remote Sens 13:352. https://doi.org/10.3390/rs13030352
Picos J, Bastos G, Daniel M, Alonso L, Armesto J (2020) Individual tree detection in a eucalyptus plantation using unmanned aerial vehicle (UAV)-LiDAR. Remote Sens 12:885. https://doi.org/10.3390/rs12050885
Pu Y, Xu D, Wang H, Li X, Xu X (2023) A new strategy for individual tree detection and segmentation from leaf-on and leaf-off UAV-LiDAR point clouds based on automatic detection of seed points. Remote Sens 15:1619. https://doi.org/10.3390/rs15061619
Scheeres J, de Jong J, Brede B, Brancalion PHS, Broadbent EN, Zambrano AMA, Gorgens EB et al (2023) Distinguishing forest types in restored tropical landscapes with UAV-borne LiDAR. Remote Sens Environ 290:113533. https://doi.org/10.1016/j.rse.2023.113533
Soininen V, Kukko A, Yu X, Kaartinen H, Luoma V, Saikkonen O, Holopainen M, Matikainen L, Lehtomäki M, Hyyppä J (2022) Predicting growth of individual trees directly and indirectly using 20-year bitemporal airborne laser scanning point cloud data. Forests 13:2040. https://doi.org/10.3390/f13122040
Straker A, Puliti S, Breidenbach J, Kleinn C, Pearse G, Astrup R, Magdon P (2023) Instance segmentation of individual tree crowns with YOLOv5: A comparison of approaches using the ForInstance benchmark LiDAR dataset. ISPRS Open J Photogramm Remote Sens 9:100045. https://doi.org/10.1016/j.ophoto.2023.100045
Strîmbu VF, Strîmbu BM (2015) A graph-based segmentation algorithm for tree crown extraction using airborne LiDAR data. ISPRS J Photogramm Remote Sens 104:18. https://doi.org/10.52638/rfpt.2015.555
Stroner M, Urban R, Kremen T, Braun J (2023) UAV DTM acquisition in a forested area—Comparison of low-cost photogrammetry (DJI Zenmuse P1) and LiDAR solutions (DJI Zenmuse L1). Eur J Remote Sens 56:2179942. https://doi.org/10.1080/22797254.2023.2179942
Sun C, Huang C, Zhang H, Chen B, An F, Wang L, Yun T (2022) Individual tree crown segmentation and crown width extraction from a heightmap derived from aerial laser scanning data using a deep learning framework. Front Plant Sci 13:914974. https://doi.org/10.3389/fpls.2022.914974
Sun Z, Wang Y-F, Ding Z-D, Liang R-T, Xie Y-H, Li R, Li H-W, Pan L, Sun Y-J (2023) Individual tree segmentation and biomass estimation based on UAV digital aerial photograph. J Mt Sci 20(3):724–737. https://doi.org/10.1007/s11629-022-7563-7
Torresan C, Carotenuto F, Chiavetta U, Miglietta F, Zaldei A, Gioli B (2020) Individual tree crown segmentation in two-layered dense mixed forests from UAV LiDAR data. Drones 4:10. https://doi.org/10.3390/drones4020010
Wallace L, Lucieer A, Watson C, Turner D (2012) Development of a UAV-LiDAR system with application to forest inventory. Remote Sens 4:1519–1543. https://doi.org/10.3390/rs4061519
Wang D, Kankare V, Puttonen E, Hollaus M, Pfeifer N (2017) Reconstructing stem cross section shapes from terrestrial laser scanning. IEEE Geosci Rem Sen M 14(2):272–276. https://doi.org/10.1109/LGRS.2016.2638738
White JC, Tompalski P, Vastaranta M, Wulder MA, Saarinen N, Stepper C, Coops NC (2017) A model development and application guide for generating an enhanced forest inventory using airborne laser scanning data and an area-based approach. 38 CWFC Information Report FI-X-018, Canadian Forest Service, Pacific Forestry Centre, Victoria, BC, Canada. http://cfs.nrcan.gc.ca/pubwarehouse/pdfs/38945.pdf
Williams J, Schönlieb C-B, Swinfield T, Lee J, Cai X, Qie L, Coomes DA (2020) 3D segmentation of trees through a flexible multiclass graph cut algorithm. IEEE T Geosci Remote 58:2. https://doi.org/10.1109/TGRS.2019.2940146
Xiang B, Wielgosz M, Kontogianni T, Peters T, Puliti S, Astrup R, Schindler K (2024) Automated forest inventory: Analysis of high-density airborne LiDAR point clouds with 3D deep learning. Remote Sens Environ 305:114078. https://doi.org/10.1016/j.rse.2024.114078
Xiao W, Zaforemska A, Smigaj M, Wang Y, Gaulton R (2019) Mean shift segmentation assessment for individual forest tree delineation from airborne lidar data. Remote Sens 11:1263. https://doi.org/10.3390/rs11111263

Yan W, Guan H, Cao L, Yu Y, Gao S, Lu J (2018) An automated hierarchical approach for three-dimensional segmentation of single trees using UAV LiDAR data. Remote Sens 10:1999. https://doi.org/10.3390/rs10121999
Yan Y, Lei J, Jin J, Shi S, Huang Y (2024) Unmanned aerial vehicle–light detection and ranging-based individual tree segmentation in Eucalyptus spp. forests: Performance and sensitivity. Forests 15:209. https://doi.org/10.3390/f15010209
You L, Tang S, Song X, Lei Y, Zang H, Lou M, Zhuang C (2016) Precise Measurement of Stem Diameter by Simulating the Path of Diameter Tape from Terrestrial Laser Scanning Data. Remote Sens 8:717. https://doi.org/10.3390/rs8090717
Yu J, Lei L, Li Z (2024) Individual tree segmentation based on seed points detected by an adaptive crown shaped algorithm using UAV-LiDAR data. Remote Sens 16:825. https://doi.org/10.3390/rs16050825
Zhang Y, Wang X (2021) Geographical spatial distribution and productivity dynamic change of eucalyptus plantations in China. Sci Rep 11:19764. https://doi.org/10.1038/s41598-021-97089-7
Zhang Z, Cao L, Mulverhill C, Liu H, Pang Y, Li Z (2019) Prediction of diameter distributions with multimodal models using LiDAR data in subtropical planted forests. Forests 10:125. https://doi.org/10.3390/f10020125
Zhang B, Li X, Du H, Zhou G, Mao F, Huang Z, Zhou L et al (2022) Estimation of urban forest characteristic parameters using UAV-Lidar coupled with canopy volume. Remote Sens 14:6375. https://doi.org/10.3390/rs14246375
Zhang W, Cen J, Feng J, Tan C, Huang X (2022b) Study on binary volume model for Eucalyptus based on tree height and crown width in Guangxi. Guangxi Sci 29(4):785–792. https://doi.org/10.13656/j.cnki.gxkx.20220919.021